Final Report

STATISTICAL EVALUATION OF GLOBAL PRECIPITATION ESTIMATES OVER DATA SCARCE WESTERN HIMALAYAN REGION OF INDIA

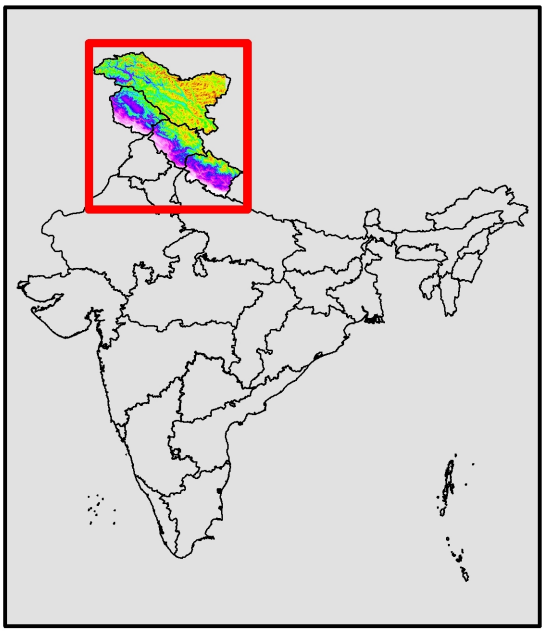

Western Himalayan Regional Centre, Jammu

National Institute of Hydrology

October 2021

Director

Dr. J.V. Tyagi

Head & Coordinator

Dr. M.K. Goel

Study Group

Dr. D.S. Bisht (Scientist 'B')

Dr. S.S. Rawat (Scientist 'E')

Dr. P.G. Jose (Scientist 'E')

Abstract

Precipitation is one of the most important meteorological variables in hydrological studies which has maximum influence on the overall outcome. In Western Himalayan Region (WHR), owing to the complex terrain and rugged topography it is difficult to find weather observatories in dense network. Moreover, even if the dense network can be ensured in future, the problem of past record will still persist. In hydrological modelling or climatology, past records are extremely important as they helps in analysing the change in the local hydrological regime. With the advent of numerous global satellite products in the recent decades dependability of hydrologists has lessened on the station data as the global precipitation estimates (GPEs) can be readily availed and utilized. Since the accuracy or skills of GPEs may differ from region to region, it is vital to analyse their ability in resolving the regional precipitation climatology using appropriate statistical methods. In this study, a total of five GPEs, viz., APHRODITE, PERSIANN-CDR, CHIRPS, CMORPH, and IMERG were evaluated for their abilities in resolving regional precipitation climatology of WHR with respect to gridded precipitation product of India Meteorological Department (IMD). Different performance indicators i.e., Probability of Detection (POD), False Alarm Ratio (FAR), Normalised Root Mean Sqaure Deviation (NRMSD), Pearson Correlation Coefficient (CC) and Skill Score (SS) were used for evaluating the GPEs. Multicriterion Decision Making (MCDM)approaches i.e., Compromise Programming (CP), Cooperative Game Theory (CGT), Technique for Order of Preference by Similarity to Ideal Solution (TOPSIS), Weighted Average Technique (WAT), and Fuzzy TOPSIS were used for ranking the GPEs across different grids in WHR. Entropy based weight assignment to NRMSD, CC, and SS were performed while applying them in MCDM methods. Group Decision Making (GDM) approach utilizing spearman correlation coefficient and additive ranking rule was employed to obtain the final ranking of GPEs from multiple rankings assigned through different MCDM methods. The GPEs were ranked for daily precipitation, monthly precipitation, and monthwise

dsily precipitation across all the grids. Overall, APHRODITE is found to perform better than other GPEs in majority of the grids whereas CHIRPS and CMORPH were found to be least favourable products among the five GPEs for majority of the grids. Methodology and results elaborated in detail in the report.

Keywords: Western Himalayan Region, Global Precipitation Estimates, Multicriterion Decision Making, Group Decision Making

Contents

List of Figures

List of Figures

List of Tables

List of Abbreviations

APHRODITE	Asian Precipitation - Highly-Resolved Observational Data Integration Towards Evaluation
CC	Pearson Correlation Coefficient
CGT	Cooperative Game Theory
CHIRPS	Climate Hazards Group InfraRed Precipitation with Station data
CMORPH	Climate Prediction Center morphing method
CP	Compromised Programming
FAR	False Alarm Ratio
GDM	Group Decision-making
GPE	Global Precipitation Estimate
GPM	Global Precipitation Measurement
IMD	India Meteorological Department
IMERG	Integrated Multi-satellitE Retrievals for GPM
MCDM	Multicriterion Decision-making
NRMSD	Normalized Root Mean Square Deviation
PERSIANN-CDR	Precipitation Estimation from Remotely Sensed Information using Artificial Neural Networks- Climate Data Record
POD	Probability of detection
SS	Skill Score

TOPSIS	Technique for Order Preference by Similarity to an Ideal Solution
WAT	Weighted Average Technique

Chapter 1

Introduction

1.1 Background

Western Himalayan Region (WHR) of India, that mainly covers Jammu & Kashmir, Ladakh, Himachal Pradesh, and Uttarakhand, houses most of the Indian glaciers feeding water to most of the rivers of flowing through Ganga and Indus basin. In recent years, numerous flood events have been reported in the WHR along with the drying/ depleting springs across the region (Bhadwal et al., 2017; Bisht et al., 2019; Mishra, 2015; Rawat et al., 2018; Shah, 2015). Since, it has been established that global warming has altered the precipitation regimes across the world, it is imperative to study how precipitation signatures have changed across WHR to understand it's implication on floods and depleting springs discharge. Sparsely distributed raingage networks in WHR and complex terrain coupled with harsh climatic conditions pose challenges in maintaining quality precipitation records. Therefore, data scarcity due to various reasons becomes the major obstacle in analyzing the precipitation dynamics vis-à-vis changing climate.

With advancement in technology, the manual intervention and station based data recording has been overcome to a greater extent wherein an array of precipitation products were developed by researchers across the globe using sophis-

ticated techniques have been made available to the scientific community. Besides, remotely sensed precipitation products are further available over the past few years from the satellite based observations. Open available global precipitation dataset are easily accessible and have been widely used in a number of studies (Beria et al., 2017; Bharti et al., 2016; Ciabatta et al., 2016; Nanda et al., 2016; Parida et al., 2017; Wu et al., 2018). Though the importance of station observations cannot be ignored, global precipitation estimates are useful in understanding the retrospective climate and its evolution with time and aid in real time applications.

1.2 Problem Definition

Precipitation is an essential input for the Indian agricultural production, water supply, and livelihood. However, accurate quantification of precipitation at the sub-regional and local scale is considered as a challenging task owing to its erratic behavior and skewed statistics (Meher et al., 2017). The study of rainfall change scenario over the Himalayan region is very important as the livelihood of more than half a billion people and the vast biodiversity of India highly depend on meltwater from the Himalayas (Meher et al., 2017). However, the accurate estimation of climate change information over Himalayan region remains difficult because of its complex topography, sparse data availability, and poor data quality (Andermann et al., 2011; Arora et al., 2006; Bhutiyani et al., 2007; Dimri & Dash, 2012; Palazzi et al., 2013; Singh et al., 2009, 1995). In climate change studies it is required to have long term record of rainfall for applying various statistical tests. These long-term records are required to obtain robust estimates of distribution parameters such as scale, shape, and location parameters to use in quantile mapping, frequency analysis etc. Therefore, it is imperative to employ the long term time series instead of satellite rainfall information available at shorter interval. Different precipitation products are available for different time frames and one single global precipitation products rarely ensures longer time coverage. In such case, there is a need to develop a longer dataset by combining information from different products based on their skills; however, prior to that the products should be evaluated and ranked for their performance to avoid wrongful selection. Furthermore, to use any global

dataset for WHR, it is essential to assess its skills in resolving the precipitation climatology and ability in capturing extreme events over WHR. A comprehensive statistical approach has to be adopted for such evaluations. Statistical approach essentially assesses the accuracy of precipitation products in statistical terms in temporal and spatial scale.

1.3 Objectives of the study

The present study aims to evaluate various available global datasets or global precipitation estimates (GPEs) for WHR and rank them as per their skills in resolving the precipitation climatology. Keeping this in view, the following objectives were laid for the study,

1. Spatial and temporal aggregation of various global precipitation estimates to compare with IMD gridded precipitation product.
2. Statistical evaluation of global precipitation estimates to assess their skills in resolving regional precipitation climatology and extreme events .
3. Identification of suitable GPEs through performance ranking for WHR employing Multicriterion Decision Making and Group Decision Making approaches.

1.4 Chapterization

This report is structured and organized into five chapters as follows,

Chapter-1 presents an overview of the study, problem statement and specifies the major objectives. It also summaries the organization of the report.

Chapter-2 provides the description of study area i.e., Western Himalayan Region (WHR) and its climatology. It also discusses the various data i.e., Global

Precipitation Estimates (GPE) and observed gridded precipitation product developed by India Meteorological Data (IMD) in context of study area.

Chapter-3 describes the methodology and various performance indicators used in the study for statistical evaluation of GPEs and their ranking for the study area. It provides the description on Multi Criteria Decision Making (MCDM) and Group Decision Making (GDM) for obtaining the ranks based on different performance criterion.

Chapter-4 presents the results of analysis pertaining to GPEs ranking and their evaluation in detail with figures, spatial maps, and tables.

Chapter-5 summarizes the report in brief and presents the key conclusion drawn from the study. It also presents the limitation of the present work and scope for future study.

Chapter 2

Study Area and Data Used

2.1 Description of Study area

The climate of Western Himalayan Region (WHR) varies from tropical at the base of the mountains to permanent ice and snow at the highest elevations (Das et al., 2018). Glaciers from the high mountains of this region are a source of water for the rivers flowing from this area to lower basins. Indus and Ganges are the two most important river systems, others are Jhelum, Chenab, Ravi, Beas and Sutlej prevails over this region. The diversity of the climate in this region is the by-product of the variation in latitude, longitude and altitude. Physiography conditions divide the whole WHR broadly into Shivalik Hills (Punjab, Haryana, UK, HP and part of erstwhile J & K), Lower or lesser Himalaya (Dhauladhar range, Pirpanjal range and Southern part of Kumaon and Garhwal Himalaya), Great Himalaya (north of Kashmir valley, Pangi Valley and northern parts of Kumaon and Garhwal Himalaya) and Trans Himalaya (including Karakoram, Ladakh and Zanskar ranges). The presence of the WHR in the north of India is considered as an important source for generating and maintaining the climate over the entire northern belt of the Indian subcontinent. The WHR experiences four distinct seasons, namely winter (DJF), pre-monsoon (MAM), monsoon (JJAS) and post-monsoon (ON). Fifty to sixty percentage of total annual rainfall is received during

2.1. Description of Study area

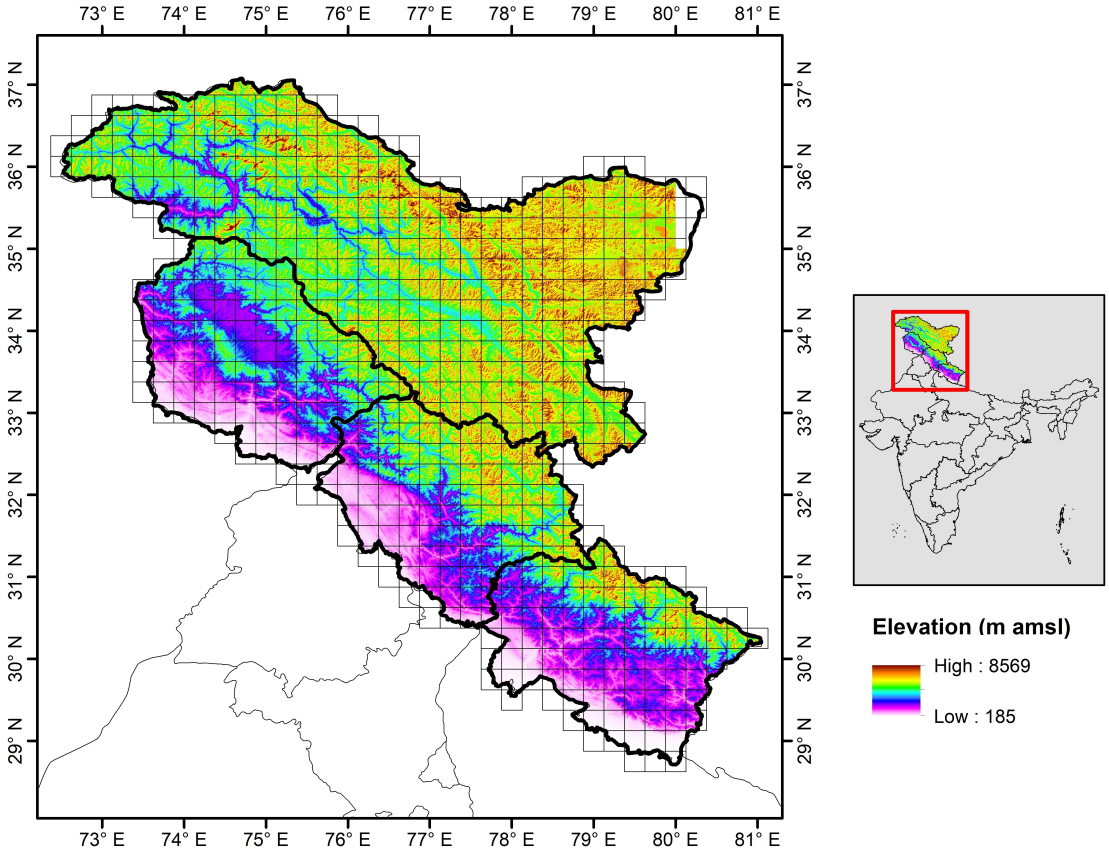

Figure 2.1: Elevation variation using SRTM 90 m DEM in western Himalayan region (Quarter degree grids for which IMD provides gridded rainfall are overlaid)

the monsoon season and the rest is received in the winter season during which rainfall is largely influenced by the western disturbances. The topography of WHR has a huge variability which ranges from $\sim$ 186 m amsl to $\sim$ 8569 m amsl (Figure 2.1).

Characteristics of observed rainfall distribution over the WHR have been studied extensively (Arora et al., 2006; Basistha et al., 2008, 2009; Bhutiyani et al., 2010; Dimri & Dash, 2012; Kripalani et al., 2003; Singh & Kumar, 1997). Over the whole WHR of India, the annual and monsoon rainfall has shown a significant negative trend during 1866–2006 (Bhutiyani et al., 2010). A small part of the WHR (i.e., the Uttarakhand subdivision) has also shown a negative trend in the annual and monsoon rainfall during the last century (Basistha et al., 2009; Singh

& Mal, 2014). The annual rainfall over some point locations, namely, Handwara, Kulgam, and Srinagar stations of Kashmir valley, also experienced negative trends during 1903–82 (Jain & Kumar, 2012). Similarly, a study by (Guhathakurta & Rajeevan, 2008) reported that the premonsoon rainfall over WHR has shown a positive trend over WHR during 1901–2003. On the other hand, some studies (Bhutiyani et al., 2010; Khan, 2001; Shrestha et al., 2000) indicated winter rainfall has shown positive trends in the last century while other studies (Dimri & Dash, 2012; Shekhar et al., 2010) reported negative trends in the recent decades over WHR.

During the winter season, the WHR region receives precipitation in the form of rainfall and snow, which is caused by extratropical storms known as western disturbances (WD), which tend to develop over the Mediterranean Sea and Atlantic Ocean and move eastward (Azadi et al., 2002; Bhutiyani et al., 2010; Dimri & Ganju, 2007; Dimri, 2012; Dimri et al., 2015; Shekhar et al., 2010). The intraseasonal variability of winter rainfall over the western Himalayan region is also influenced by the northwest propagation of lower-tropospheric air (850 hPa) from the equatorial Indian Ocean (Dimri et al., 2016). During the monsoon season, WHR receives rainfall from the large-scale monsoonal circulation that moves east–west. The amount of precipitation has shown a gradually decreasing trend from east to west mostly as a result of increasing distance from the source region of the Bay of Bengal (Bhatt & Nakamura, 2005).

A vast variation in elevation from mean seal elevation that ranges from 200 m amsl to 8500 m amsl in WHR makes the topography very complex. This also posed challenges in terms of having dense raingauge network to capture the rainfall variability across the space. Some of the places in WHR are very difficult to maneuver due to harsh terrain and cold weather. Majority of the Himalayan population in western Himalayan region resides in the areas having mean sea elevation below 3000 m. Area above this elevation level less affected by anthropogenic activities.

The grids having mean elevation below 3000 m amsl can be seen in (Figure 2.2), which can be distinguished by the color scheme. The grids shown in 'red'

2.1. Description of Study area

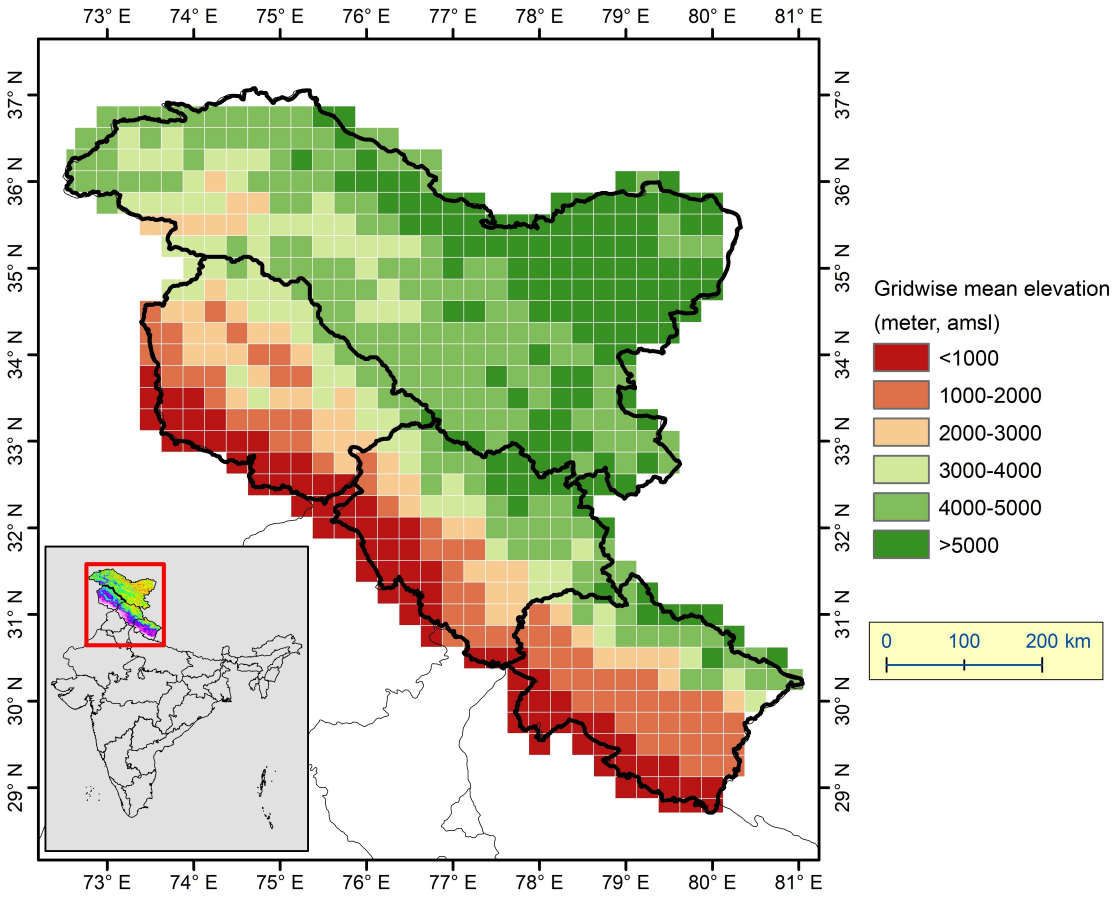

Figure 2.2: Gridwise mean elevation (from mean sea level) estimated using SRTM 90m DEM

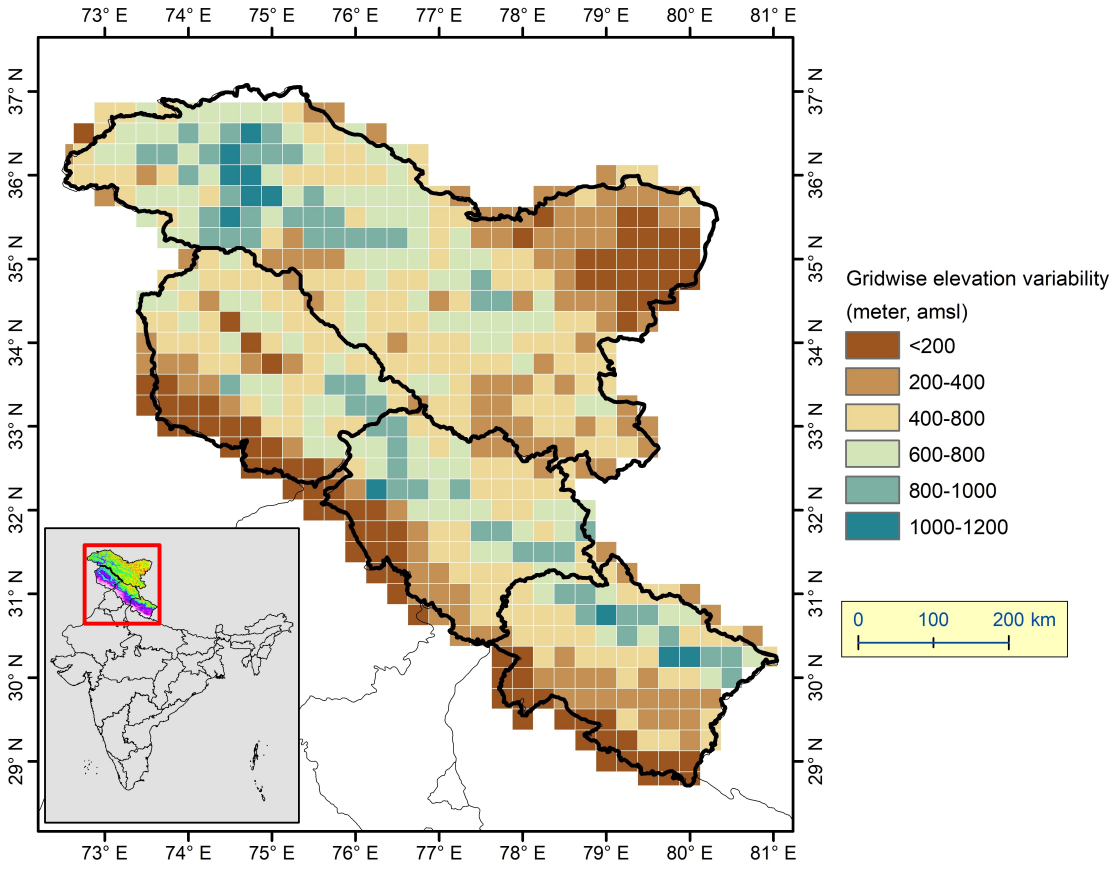

Figure 2.3: Gridwise variation in elevation estimated using SRTM 90m DEM

are most favorable for human habitats nonetheless, the terrain is still complex in comparison to plain regions especially for the grids having mean elevation between 1000-3000 m amsl. The complexity of the terrain can be seen by the variation in elevation level within the grids (Figure 2.3) that ranges from <200 m to >1000 m.

2.2 Description of Data Used

2.2.1 Global Precipitation Estimates

Some of the widely used open datasets from various sources are as follows, CHIRPS, PERSIANN-CDR, APHRODITE, CMORPH, and IMERG. These datasets cover different time frames (Table 2.1) and have been developed using different techniques/ algorithms.

Table 2.1: Description of various datasets (global precipitation estimates) used in the study

SI. No.	Dataset	Availability	Spatial Resolution	Temporal Resolution
1	APHRODITE	Jan 1951 - Dec 2007 Jan 2007 - Dec 2015	0.25° x 0.25°	Daily
2	PERSIANN-CDR	Jan 1983 - Dec 2017	0.25° x 0.25°	Daily
3	CHIRPS	Jan 1981 - May 2019	0.25° x 0.25°	Daily
4	CMORPH	Dec 2002 - Oct 2017	0.25° x 0.25°	Daily, Sub-daily
5	IMERG	Jan 2000 - Present	0.10° x 0.10°	Daily, Sub-daily

2.2.1.1 APHRODITE

APHRODITE's (Asian Precipitation - Highly-Resolved Observational Data Integration Towards Evaluation) daily gridded precipitation is the only long-term (1951 onward) continental-scale daily product that contains a dense network of

daily rain-gauge data for Asia including the Himalayas, South and Southeast Asia and mountainous areas in the Middle East. The number of valid stations was between 5000 and 12,000, representing 2.3 to 4.5 times the data available through the Global Telecommunication System network, which were used for most daily grid precipitation products. The initial purpose of APHRODITE was to formulate reliable, rain gauge–based, high-resolution products. These were for validating high-resolution climate model simulations and for statistical downscaling of relatively course climate simulation outputs, to make localized precipitation forecasts according to future climate change resulting from the anthropogenic greenhouse effect. APHRODITE products are used for such purposes because they contain substantial rain gauge data and use an interpolation method that considers orographic effects. Hence, they represent a useful database for transforming biased model precipitation patterns into more realistic ones, especially in mountainous areas.

2.2.1.2 PERSIANN-CDR

The Precipitation Estimation from Remotely Sensed Information using Artificial Neural Networks- Climate Data Record (PERSIANN-CDR) provides daily rainfall estimates at a spatial resolution of 0.25° in the latitude band 60S-60N from 1983 to the near-present. The precipitation estimate is produced using the PERSIANN algorithm on GridSat-B1 infrared satellite data, and the training of the artificial neural network is done using the National Centers for Environmental Prediction (NCEP) stage IV hourly precipitation data. The PERSIANN-CDR is adjusted using the Global Precipitation Climatology Project (GPCP) monthly product version 2.2 (GPCPv2.2), so that the PERSIANN-CDR monthly means degraded to 2.5° spatial resolution match GPCPv2.2. PERSIANN CDR is a Climate Data Record, which the National Research Council (NRC) defines as a time series of measurements of sufficient length, consistency, and continuity to determine climate variability and change.

2.2.1.3 CHIRPS

Climate Hazards Group InfraRed Precipitation with Station data (CHIRPS) is a 30+ year quasi-global rainfall dataset. Spanning 50°S-50°N (and all longitudes), starting in 1981 to near-present, CHIRPS incorporates 0.05° resolution satellite imagery with in-situ station data to create gridded rainfall time series. CHIRPS uses the Tropical Rainfall Measuring Mission Multi-satellite Precipitation Analysis version 7 (TMPA 3B42 v7) to calibrate global Cold Cloud Duration (CCD) rainfall estimates. CHIRPS uses a 'smart interpolation' approach, working with anomalies from a high resolution climatology. CHIRPS incorporates station data in a two phase process, producing two unique products. In the first phase, which yields a preliminary rainfall product with 2-day latency, sparse World Meteorological Organization's Global Telecommunication System (GTS) gauge data are blended with CCD-derived rainfall estimates at every pentad. There are six pentads in a calendar month, five 5-day pentads and one pentad with the remaining 3 to 6 days of the month. In the second phase, which yields a final product with a $\sim$ 3 week latency, the best available monthly (and pentadal) station data are combined with monthly (and pentadal) high resolution CCD-based rainfall estimates to produce fields that are similar to gridded monthly station products like those produced by the Global Precipitation Climatology Centre (GPCC), or University of East Anglia's Climate Research Unit (CRU). Thus, the CHIRPS falls somewhere between heavily curated interpolated gauge datasets like the GPCC and sparse gauge plus satellite products like the RFE2.

2.2.1.4 CMORPH

These satellite precipitation estimates are reprocessed and bias corrected, to form a CDR of high resolution global precipitation analysis. The bias-corrected CMORPH CDR processing system generates bias-corrected, integrated satellite precipitation estimates over the global domain. The production of the output precipitation fields are a combination of three different time-space resolutions to accommodate user requirements of various backgrounds. The CMORPH satellite precipitation

estimates are created in two steps. First, the purely satellite-based global fields of precipitation are constructed through integrating Level 2 retrievals of instantaneous precipitation rates from all available passive microwave measurements aboard low earth orbiting platforms. Bias in these integrated satellite precipitation estimates is then removed through comparison against CPC daily gauge analysis over land and adjustment against the Global Precipitation Climatology Project (GPCP) merged analysis of pentad precipitation over ocean. The bias corrected CMORPH satellite precipitation estimates are created on an 8×8 km grid over the global domain from 60S–60N and in a 30-minute interval from January 1, 1998. Due to the delay of some input data sets, this formal version (Version 1) bias corrected CMORPH is produced manually once a month at a latency of 3-4 months.

2.2.1.5 IMERG

The Global Precipitation Measurement (GPM) mission is an international network of satellites that provide the next-generation global observations of rain and snow. Building upon the success of the Tropical Rainfall Measuring Mission (TRMM), the GPM concept centers on the deployment of a "Core" satellite carrying an advanced radar / radiometer system to measure precipitation from space and serve as a reference standard to unify precipitation measurements from a constellation of research and operational satellites. Through improved measurements of precipitation globally, the GPM mission is helping to advance our understanding of Earth's water and energy cycle, improve forecasting of extreme events that cause natural hazards and disasters, and extend current capabilities in using accurate and timely information of precipitation to directly benefit society. GPM, initiated by NASA and the Japan Aerospace Exploration Agency (JAXA) as a global successor to TRMM, comprises a consortium of international space agencies, including the Centre National d'Études Spatiales (CNES), the Indian Space Research Organization (ISRO), the National Oceanic and Atmospheric Administration (NOAA), the European Organization for the Exploitation of Meteorological Satellites (EUMETSAT), and others.

The GPM Core Observatory carries the first space-borne Ku/Ka-band Dual-frequency Precipitation Radar (DPR) and a multi-channel GPM Microwave Imager (GMI). The DPR instrument, which provides three dimensional measurements of precipitation structure over 78 and 152 mile (125 and 245 km) swaths, consists of a Ka-band precipitation radar (KaPR) operating at 35.5 GHz and a Ku-band precipitation radar (KuPR) operating at 13.6 GHz. Relative to the TRMM precipitation radar, the DPR is more sensitive to light rain rates and snowfall. In addition, simultaneous measurements by the overlapping of Ka/Ku-bands of the DPR can provide new information on particle drop size distributions over moderate precipitation intensities.

2.2.2 IMD Observed Gridded Precipitation

India Meteorological Department (IMD) provides high resolution ($0.25° \times 0.25°$) gridded precipitation product. This product is available for the longer time period starting from 1901 to 2019 over the mainland India and have been used widely in research focusing on climatology (Bisht et al., 2018, 2019; Meher et al., 2017) satellite rainfall evaluation (Banerjee et al., 2020; Beria et al., 2017). The IMD gridded product is developed using daily rainfall records from 6995 rain gauge stations across the country after quality control (Pai et al., 2014). However, these numbers varies from year to year based on the number of operational rain gauge station. In Himalayas, there is undulating topography, and paucity of ground based observatory (rain-gauge and radar network) are very sparse to get accurate measurements of rainfall information. In particular, it is important to mention the deficit of observatories beyond 2000 m. The observations at higher Indian Himalayan region is very sparse and simultaneously influence from and to other neighbouring nations at large scale in the IMD observation is inhibited (Banerjee et al., 2020).

Majority of the WHR is not covered by IMD raingauge network as shown in Figure 2.4. Area at high altitude, i.e., greater Himalayas, is not covered and the raingauge density in lesser Himalayas is very poor (Figure 2.4a, b, and c).

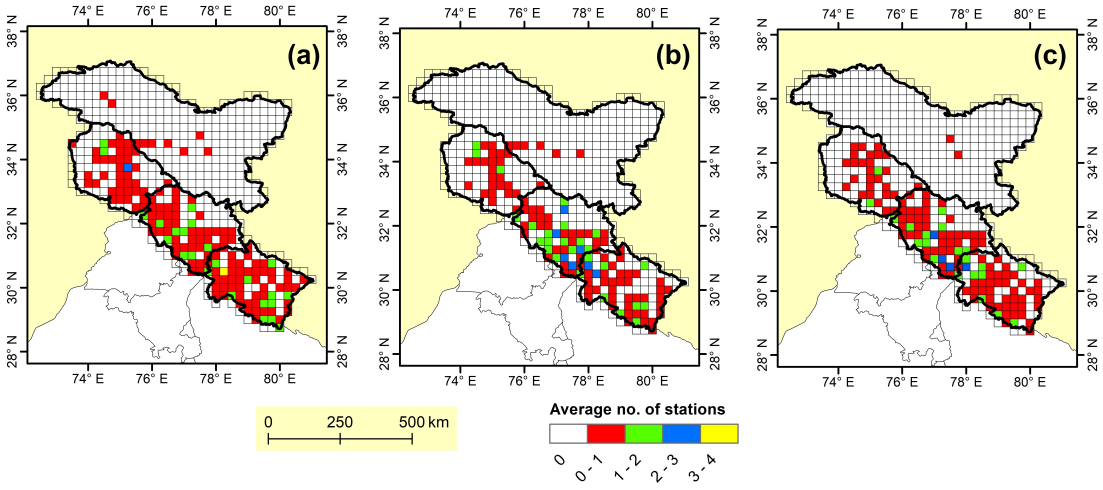

Figure 2.4: Gridwise average number of rainfall stations used in preparation of IMD gridded dataset for the period of (a) 1901-2016, (b) 1976-2005 (c) 1987-2016

Majority of the grids show that data from 0-1 raingauge station is on an average over the period of time for creating the gridded dataset. It is worth noting that in these grids raingauge stations were not functional in some of the years as observed from the data while extracting the information illustrated in Figure 2.4.

Overall, the number of total raingauge station used in creating IMD gridded rainfall product has decreased over the period of time in comparison to large number of raingauge station used during 1950-1975. In climate studies often 30 years of data for the period of 1976-2005 is required to perform statistical downscaling and bias-correction as many of the GCMs in CMIP5 has simulate retrospective climate till year 2005. The latest CMIP6 projection provides the historical simulation till year 2014 (Papalexiou et al., 2020), which further highlights the need of good quality observation climatological records for climate studies.

Apparently, a decline in the raingauge network in the WHR can be seen in this period (i.e., 1976-2005, Figure 2.5) which might have reflected poorly in IMD gridded rainfall product.

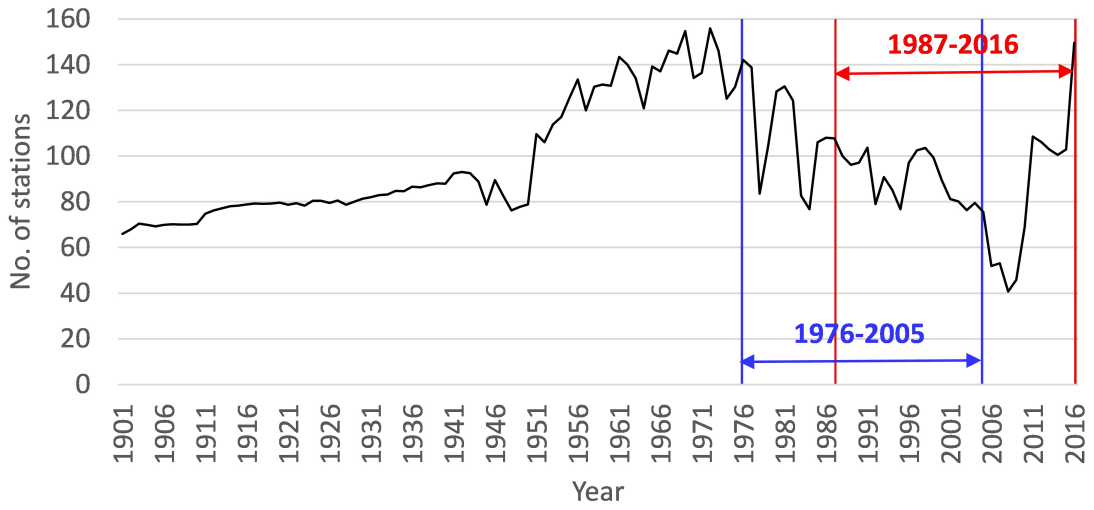

Figure 2.5: Yearwise total number of rainfall station used for preparation of IMD gridded rainfall

Similarly, last 30 years of record is important to analyze the recent climatic window vis-à-vis water resource dynamics of the region. Though improvement in raingaguge density is observed year 2008 onwards (Figure 2.5), majority of years are marred by poor raingauge density. Therefore, it is imperative to find the alternative of IMD data for better interpretation of regional precipitation climatology.

Chapter 3

Methodology

Global precipitation estimates (GPEs) from various datasets can be evaluated using suitable statistical techniques for their efficacy vis-a-vis specific region. However, besides providing the statistical evaluation, it is also crucial to perform the ranking of these products while considering different statistical criterion to gain more insight regarding their utility. This calls for the need of multicriterion decision-making (MCDM) approach to incorporate different statistical attributes of these GPEs and Group decision-making (GDM) approaches to obtain their overall ranking based on their performance.

In subsequent sections detail about performance indicators, MCDM and GDM based ranking approaches are discuss in detail.

3.1 Performance indicator

To evaluate the ability of global climatological data in resolving the regional or local scale climatology, appropriate performance indicators should be utilized. In the context of present study, the performance indicator is a measure of any global precipitation estimate in capturing the behaviour of precipitation as produced by observed gridded record. Pearson correlation coefficient (CC), Percentage bias

(PBIAS), Probability of detection (POD), False alarm ratio (FAR), Nash–Sutcliffe efficiency (NSE), Root mean square error (RMSE), Skill score (SS), Mean Absolute Error (MAE), Relative bias (RBIAS) are some of the commonly employed performance indicator to evaluate the satellite rainfall vis-a-vis observed records (Beria et al., 2017; Chowdhury et al., 2021; Shukla et al., 2019).

In this report, POD and FAR were employed to detect how well the selected GPEs capture the light, moderate and heavy precipitation across the region following Beria et al. (2017). It was found that 50, 75, and 99 percentile threshold rainfall values roughly fall in the range of light (2.5 to 7.5 mm per day), moderate (7.6 to 35.5 mm per day), and heavy rainfall (64.5 to 124.4 mm per day) criteria of IMD (https://www.imdpune.gov.in/Weather/Reports/glossary.pdf, accessed on May 2021). Therefore, the POD and FAR for the selected GPEs were estimated for 50, 75 and 99 percentile rainfall values of IMD gridded precipitation at respective grids. Expression for computing POD and FAR are presented in Table 3.1 and contingency table to compute POD and FAR is provided in Table 3.2.

Chowdhury et al. (2021) reported that no specific evidence are available in favour of any specific performance indicators therefore, based on the users' discretion appropriate indicators can be chosen for evaluation. Therefore, apart from using POD and FAR, three other performance indicators, viz., normalised root mean square deviation (NRMSD), correlation coefficient (CC) and skill score (SS) were employed (Table 3.1) for skill evaluation and performance ranking of GPE following Srinivasa Raju & Nagesh Kumar (2015a). These three indicators, i.e., NRMSD, CC, and SS are easy to interpret and appropriate for such evaluations and represent the difference, strength of linear association, and similarity between the probability distribution function of reference and targeted time series, respectively. These three indicators were employed in MCDM analysis, which is discussed in detail in section 3.2.3.

Table 3.1: Summary of performance indicators used to evaluate the GPEs

Indicator	Mathematical expression	Range	Remark
POD	$\frac{HIT}{HIT+MISS}$	$\in$ [0,1]	Best value is 1, worst value is 0
FAR	$\frac{FALSE}{HIT+FALSE}$	$\in$ [0,1]	Best value is 0, worst value is 1
NRMSD	$\frac{\sqrt{\frac{1}{N}\sum_{i=1}^{N}(obs_i - mod_i)^2}}{\overline{obs}}$	$\in$ [0 , ∞)	Smaller value is favourable.
CC	$\frac{\sum_{i=1}^{N}\left(obs_i - \overline{obs}\right)\left(mod_i - \overline{mod}\right)}{(N-1)\sigma_{obs}\sigma_{mod}}$	$\in$ [-1,1]	Best value is 1, worst value is -1
SS	$\frac{1}{N}\sum_{i=1}^{nb}\min\left(f_{mod}f_{obs}\right)$	$\in$ [0,1]	Best value is 1, worst value is 0

N is the length of dataset.
obs_i and mod_i are the observation and modeled (GPE estimate, in present context) values, respectively.
$\overline{obs}$ and $\overline{mod}$ are the mean of observed and modeled values, respectively.
σ_{obs} and σ_{mod} are the standard deviation of observed and modeled values, respectively.
nb is the number of bins for calculating the probability density function for specific grid or region, and f_{mod} and f_{obs} are the frequencies of values in a specific bin from the modeled and observed dataset, respectively.
Contingency table for POD and FAR computation is provided in Table 3.2.

Table 3.2: Contingency table to calculate POD and FAR at specific threshold

		Modeled	
		Threshold	$\leq$ Threshold
Observed	Threshold	HIT	FALSE
	$\leq$ Threshold	MISS	NEGATIVE

3.2 Application of MCDM and GDM for performance ranking

Multicriterion Decision-Making (MCDM) aids in analysing complex problems that involves different evaluation criterion and multiple alternatives. The MCDM approach is used in present study as multiple alternatives (i.e., GPEs) were compared for their performance based on different criterion i.e., performance indicators. Out of five performance indicators shown in Table 3.1, NRMSD, CC, and SS were used to rank each GPE based on different MCDM approaches explained in section 3.2.3 and 3.2.4.

Normalization of indicators and weight determination for different criterion is required as different indicators might target different attributes and represent conflicting criteria. Different normalization techniques used in this report are presented in section 3.2.1. Relative importance or weight determination for different criterion is briefly discussed in section 3.2.2.

In the presence of multiple decision-makers, it becomes imperative to integrate the outcome of each decision-makers to obtain the final results. Group decision-making (GDM) helps in integrating the multiple decision-making criterion by analysing rank correlation and suitable rank combining rules. Section 3.2.5 briefly discuss the GDM approach used in this study. A methodology flowchart of application of MCDM and GDM is provided in Figure 3.1.

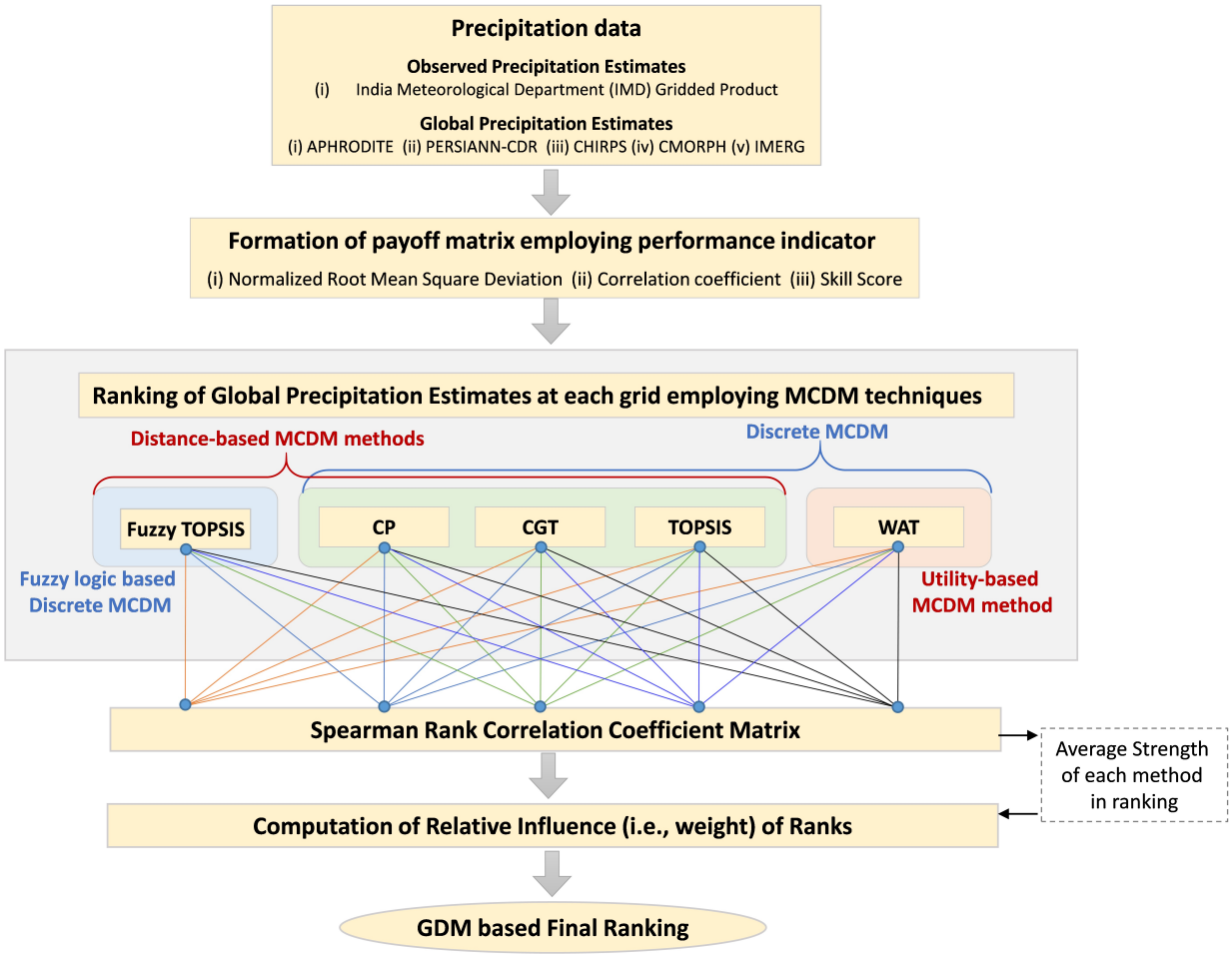

Figure 3.1: Flowchart of MCDM and GDM based GPE ranking

3.2.1 Normalization Techniques

Ranges of different performance indicators vary in different space and often cannot be compared with each other without applying appropriate statistical operation to restrict them within same space. For example, NRMSD may take any value between 0 and ∞, whereas the SS is limited to 0 and 1. Besides, depending upon the nature of datasets the values of these indicators might clustered differently. Details of different normalization techniques can be referred in Pomerol & Barba-

Romero (2000).

In this study, two types of normalization techniques, which can be termed as Norm-1 (eq. 3.1) and Norm-2 (eq. 3.2) for ease of conveying, have been employed.

$$v_i = \frac{x_i}{\sum_i^N x_i} \tag{3.1}$$

$$v_i = \frac{x_i - \min x_i}{\max x_i - \min x_i} \tag{3.2}$$

Where, v_i is the normalized vector, x_i is the value of indicator, N is the number of alternatives (i.e., GPEs in the context of present study). Normalized vector obtained using Norm-1 technique ($\in$ (0,1)) conserve the proportionality unlike Norm-2 technique ($\in$ [0,1]).

3.2.2 Weight determination using Entropy technique

In MCDM analysis, it is imperative to consider all the decision makers (i.e., performance indicators in the context of present study) to reach the final outcome. However, as different decision makers evaluate the alternative for their specific skill it is essential to assign appropriate weight or relative importance to each decision maker. There are different methods available for weight determination which can be referred in Pomerol & Barba-Romero (2000). However, in present study Entropy method was used for weight determination following Srinivasa Raju & Nagesh Kumar (2015a) and Chowdhury et al. (2021).

Though detailed description of entropy based weight determination is provided in Pomerol & Barba-Romero (2000), steps of Entropy method are explained herein for ease of understanding.

Step 1: Create the normalized payoff matrix employing Norm-1 technique

(eq. 3.1) for all the decision makers (i.e., performance indicators).

Step 2: Compute entropy for each decision maker as follows,

$$En_j = -\frac{1}{\ln(N)} \sum_{i=1}^{N} v_{ij} \ln(v_{ij}) \qquad \text{for } j = 1, \ldots, J \tag{3.3}$$

Where, En_j is the entropy for each decision maker (i.e., performance indicator or criterion), N is the number of alternatives (i.e., GPEs), i is the index of alternative, v_{ij} is the normalized value for i_{th} alternative and j_{th} decision maker.

Step 3: Compute degree of diversification D_j for each decision maker,

$$D_j = 1 - En_j \qquad \text{for } j = 1, \ldots, J \tag{3.4}$$

Step 4: Normalize the weights employing Norm-1 technique (eq. 3.1,

$$w_j = \frac{D_j}{\sum_{j=1}^{J} D_j} \tag{3.5}$$

Higher entropy value (eq. 3.3) represents higher degree of uncertainty associated with the criterion, which results into smaller degree of diversification (eq. 3.4) making the criterion less important by assigning smaller weight (eq. 3.5).

Weight determined using entropy methods were used in MCDM analysis for carrying-out performance ranking of selected GPEs as discussed in section 3.2.3 and 3.2.4.

3.2.3 Discrete Multicriterion Decision Making in deterministic scenario

In literature, there are different types of discrete MCDM analysis approaches are available in deterministic scenario. In present study, two types of Discrete MCDM methods in deterministic scenario have been employed , (i) Distance based method, and (ii) Utility based method.

Among distance based method, Compromise Programming (section 3.2.3.1), Cooperative Game Theory (section 3.2.3.2), and Technique for Order Preference by Similarity to an Ideal Solution (section 3.2.3.3) have been used. Weighted Average Technique (section 3.2.3.4) is used from various available Utility based methods.

Here it should be noted that rational of employing multiple MCDM methods for rank determination is to eventually use group decision making approach to obtain final ranking that will not only have multiple decision makers but also varying computation methods.

3.2.3.1 Compromise Programming (CP)

This methods aims to obtain the best solution which has the least distance from the ideal solution (Srinivasa Raju et al., 2017). The distance measure for finding the best solution is represented by $L_p - metric$. Steps to perform MCDM based ranking employing Compromise Programming are as follows,

Step 1: Create the normalized payoff matrix employing Norm-1 technique (eq. 3.1) for all the decision makers for weight computation.

Step 2: Find ideal value for each decision maker j among available alternatives, i.e., for CC and NRMSD, highest and lowest value, respectively, among all the alternatives would be the ideal values.

Step 3: Compute the $L_p - metric$ for each alternative as follows,

$$L_{pi} = \left[\sum_{j=1}^{J} w_j^p \left| x_j^* - x_{ji} \right|^p \right]^{\frac{1}{p}} \qquad \text{for } i = 1, \ldots, N \tag{3.6}$$

Where, L_{pi} is the $L_p - metric$ for i_{th} alternative, w_j is the weight assigned to decision maker j, x_j^* is the ideal value for j_{th} decision maker, x_{ji} is the value of j_{th} decision maker for i_{th} alternative, N is the number of alternatives, and p is the parameter for distance metric. Following Chowdhury et al. (2021) Euclidean distance is considered by taking $p = 2$.

Step 4: Find the ranking of suitable alternative from estimated L_{pi} values. Most suitable alternative will have lowest L_{pi} and vice-versa.

3.2.3.2 Cooperative Game Theory (CGT)

In this method, unlike Compromise Programming, the best solution is one which has farthest distance from the anti-ideal solution rather than the least distance from the ideal solution (Gershon & Duckstein, 1983). Cooperative Game Theory uses geometric distance measure to obtain the ranking of various alternatives. Steps to perform MCDM based ranking employing CGT approach are as follows,

Step 1: Create the normalized payoff matrix employing Norm-1 technique (eq. 3.1) for all the decision makers for weight computation.

Step 2: Find anti-ideal value for each decision maker j among available alternatives, i.e., for CC and NRMSD, lowest and highest value, respectively, among all the alternatives would be the anti-ideal values.

Step 3: Compute the geometric distance (G) for each alternative as follows,

$$G_i = \prod_{j=1}^{J} \left| x_{ji} - x_j^{**} \right|^{w_j} \qquad \text{for } i = 1, \ldots, N \tag{3.7}$$

Where, G_i is the geometric distance for i_{th} alternative, w_j is the weight assigned to decision maker j, x_j^{**} is the anti-ideal value for j_{th} decision maker, x_{ji} is the value of j_{th} decision maker for i_{th} alternative, and N is the number of alternatives.

Step 4: Find the ranking of suitable alternative from estimated G_i values. Most suitable alternative will have highest G_i value and vice-versa.

3.2.3.3 Technique for Order Preference by Similarity to an Ideal Solution (TOPSIS)

This method aims to find the best solution considering the least distance from the ideal solution like compromise programming as well as the farthest distance from the anti-ideal solution like cooperative game theory (Opricovic & Tzeng, 2004). Steps to perform MCDM based ranking employing TOPSIS method are as follows,

Step 1: Create the normalized payoff matrix employing Norm-1 technique (eq. 3.1) for all the decision makers for weight computation.

Step 2: Find the ideal (v_i) and anti-ideal (v_{ai}) value for each decision maker as explained in sections 3.2.3.1 and 3.2.3.2, respectively.

Step 3: Compute the separation measure (Opricovic & Tzeng, 2004; Srinivasa Raju & Nagesh Kumar, 2015b) of each alternative (i.e., distance) from the ideal and anti-ideal solution, and relative closeness of alternative from ideal solution as follows,

$$DS_i^+ = \sqrt{\sum_{j=1}^{J} \left(w_j x_{ji} - w_j x_j^*\right)^2} \qquad \text{for } i = 1, \ldots, N \tag{3.8}$$

$$DS_i^- = \sqrt{\sum_{j=1}^{J} \left(w_j x_{ji} - w_j x_j^{**}\right)^2} \qquad \text{for} i = 1, \ldots, N \tag{3.9}$$

$$CR_i = \frac{DS_i^-}{DS_i^- + DS_i^+} \qquad \text{for} i = 1, \ldots, N \tag{3.10}$$

Where, DS_i^+ and DS_i^- are the separation measure from the ideal and anti-ideal solutions for i_{th} alternative, respectively; w_j is the weight assigned to decision maker j; x_j^* and x_j^{**} are the ideal and anti-ideal value for j_{th} decision maker, respectively; x_{ji} is the value of j_{th} decision maker for i_{th} alternative; N is the number of alternatives; and CR_i is the relative closeness of i_{th} alternative from the ideal solution.

Step 4: Find the ranking of suitable alternative from estimated CR_i values. Most suitable alternative will have highest CR_i value and vice-versa.

3.2.3.4 Weighted Average Technique (WAT)

Unlike, CP, CGT, and TOPSIS approaches of MCDM, Weighted Average Technique is a utility based method. In this method, utility of each alternative is computed for assigning performance ranking. Steps to perform MCDM based ranking employing WAT method are as follows,

Step 1: Create the normalized payoff matrix employing Norm-1 technique (eq. 3.1) for all the decision makers for weight computation.

Step 2: Compute the utility (U) of each alternative as follows,

$$U_i = \sum_{j=1}^{J} w_j xj \qquad \text{for } i = 1, \ldots, N \tag{3.11}$$

Where, U_i is the utility of i_{th} alternative, w_j is the weight assigned to decision maker j, x_j is the value of j_{th} decision maker for i_{th} alternative, and N is the number of alternatives.

Step 4: Find the ranking of suitable alternative from estimated U_i values.

Most suitable alternative will have highest U_i value and vice-versa.

3.2.4 Discrete Multicriterion Decision Making in fuzzy scenario

In MCDM analysis uncertainty can arise during to weight assessment of the criteria or during evaluating the alternatives with respect to specific criteria (Srinivasa Raju & Nagesh Kumar, 2010). This uncertainty can be addressed in the fuzzy scenario wherein the relative values of attributes were assigned using fuzzy numbers to perform the MCDM analysis. In this study, fuzzy TOPSIS method was employed following Chowdhury et al. (2021) and Srinivasa Raju & Nagesh Kumar (2015a). Fuzzy TOPSIS method employed in this study is explained in detail in section 3.2.4.1.

3.2.4.1 Fuzzy Technique for Order Preference by Similarity to an Ideal Solution (Fuzzy TOPSIS)

The Fuzzy TPOSIS method of MCDM works on the same principle as explained in TOPSIS (section 3.2.3.3), i.e., best solution should have least distance from the ideal solution and farthest distance from the anti-ideal solution. However, unlike TOPSIS, in Fuzzy TOPSIS the distance estimation is carried out through fuzzy logic (Yang & Hung, 2007). In this study triangular membership function (TMF) was utilized for fuzzification following Chowdhury et al. (2021), Srinivasa Raju & Nagesh Kumar (2015a) and Yang & Hung (2007) due to its simplistic nature and ease of interpretation.

A fuzzy number $\tilde{A}$ with triangular membership function is characterized by (a_1, a_2, a_3), $a_1 \prec a_2 \prec a_3$ as shown in Figure 3.2. Mathematical expression for TMF is presented in equation 3.14.

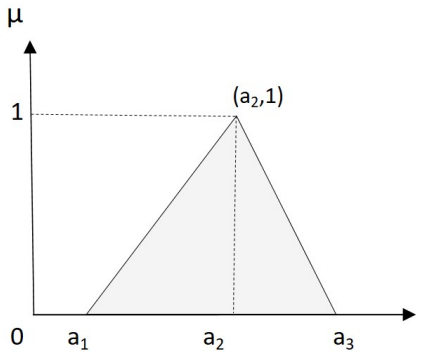

Figure 3.2: Triangular membership function for fuzzy number Ã

$$\mu_{\tilde{A}}(x) = \begin{cases} 0, & x \leqslant a_1 \\ \frac{x-a_1}{a_2-a_1}, & a_1 < x \leqslant a_2, \\ \frac{a_3-x}{a_3-a_2}, & a_2 < x \leqslant a_3, \\ 0, & x > a_3 \end{cases} \tag{3.12}$$

The distance $d(\tilde{A}, \tilde{B})$ between two fuzzy numbers $\tilde{A} = (a_1, a_2, a_3)$ and $\tilde{B} = (b_1, b_2, b_3)$ is calculated as,

$$d(\tilde{A}, \tilde{B}) = \sqrt{\frac{1}{3}\left[(a_1 - b_1)^2 + (a_2 - b_2)^2 + (a_3 - b_3)^2\right]} \tag{3.13}$$

The basic arithmetic operations between two fuzzy numbers $\tilde{A} = (a_1, a_2, a_3)$ and $\tilde{B} = (b_1, b_2, b_3)$ are as follows,

$$\tilde{A} + \tilde{B} = (a_1 + b_1,\ \ a_2 + b_2,\ \ a_3 + b_3)$$

$$\tilde{A} - \tilde{B} = (a_1 + b_3,\ \ a_2 - b_2,\ \ a_3 + b_1)$$

$$\tilde{A} \times \tilde{B} = (a_1 b_1,\ \ a_2 b_2,\ \ a_3 b_3)$$

$$\tilde{A} \div \tilde{B} = (a_1/b_3,\ \ a_2/b_2,\ \ a_3/b_1)$$

In the present study, five-level linguistic variables were used to obtain the

ranking through fuzzy logic in Fuzzy TOPSIS. To assign these linguistic variable to precise values following scheme (Table 3.3, Figure 3.3) of Yang & Hung (2007) was utilized,

Table 3.3: Linguistic variables used in triangular fuzzy membership function

Rank	Membership Function
Very Low (VL)	(0.00, 0.10, 0.25)
Low (L)	(0.15, 0.30, 0.45)
Medium (M)	(0.35, 0.50, 0.65)
High (H)	(0.55, 0.70, 0.85)
Very High (VH)	(0.75, 0.90, 1.00)

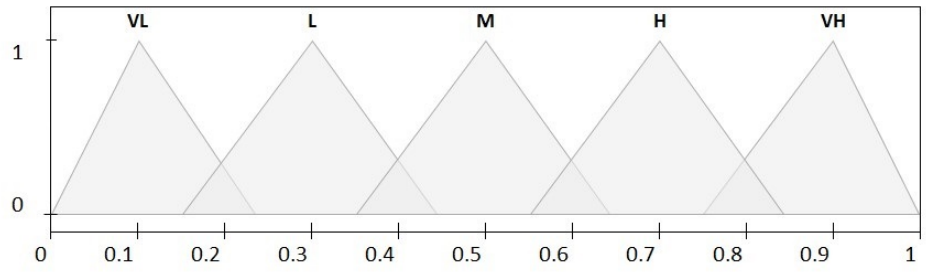

Figure 3.3: Scheme of fuzzy triangular membership scheme

$$\mu_{\tilde{A}}(x) = \begin{cases} 0, & x \leqslant a_1 \\ \frac{x-a_1}{a_2-a_1}, & a_1 < x \leqslant a_2, \\ \frac{a_3-x}{a_3-a_2}, & a_2 < x \leqslant a_3, \\ 0, & x > a_3 \end{cases} \tag{3.14}$$

Performance ranking of various alternatives using Fuzzy TOPSIS in MCDM approach can be obtained in following steps,

Step 1: Create the normalized payoff matrix employing Norm-1 technique (eq. 3.1) for all the decision makers for weight computation.

Step 2: Create the normalized payoff matrix employing Norm-2 technique (eq. 3.2) to create normalized payoff matrix to utilize in fuzzy logic. Here, Norm-2 technique is used as it provides wider range ($\in [0, 1]$) unlike Norm-1 technique which is clustered in a comparatively small range ($\in (0, 1)$). The wider range helps in utilizing all the Linguistic variables in fuzzy logic as presented in Table 3.3.

Step 3: Utilizing the triangular membership function (eq. 3.14) and Table 3.3, transform the payoff matrix (Table 3.4) into fuzzy linguistic variables (Table 3.5), as follows .

Table 3.4: Normalized payoff matrix example for Fuzzy TOPSIS analysis

	DM1	**DM2**	**DM3**
A1	0.70	0.60	0.12
A2	0.10	0.18	0.71
⋮	⋮	⋮	⋮
An	0.49	0.80	0.46
w	0.30	0.50	0.20

Table 3.5: Payoff matrix example using linguistic variables

	DM1	**DM2**	**DM3**
A1	H	M	VL
A2	VL	VL	H
⋮	⋮	⋮	⋮
An	M	H	M
w	L	M	L

Step 4: Transform Table 3.5 into fuzzy-weighted decision matrix by assigning corresponding triangular membership function to Linguistic variables in Table 3.5 from Table 3.3 and multiplying the weight (w) with each membership function.

Step 5: Compute the separation measure DS_i^+ and DS_i^- (Srinivasa Raju & Nagesh Kumar, 2010; Yang & Hung, 2007) of each alternative (i.e., distance) from the ideal, $\tilde{Y}^* = (y_1^*, y_2^*, y_3^*)$, and anti-ideal, $\tilde{Y}^{**} = (y_1^{**}, y_2^{**}, y_3^{**})$, solution following eq. 3.13. Here, ideal and anti-ideal values are $\tilde{v}_i = (1, 1, 1)$ and $\tilde{v}_{ai} = (0, 0, 0)$, respectively.

Step 6: Compute the relative closeness CR_i of alternative from ideal solution using eq. 3.10.

Step 7: Find the ranking of suitable alternative from estimated CR_i values. Most suitable alternative will have highest CR_i value and vice-versa.

3.2.5 Group Decision Making

In group decision making approach, the ranking provided by different ranking approaches are integrated to obtain the most acceptable ranking rather than relying on the results of one single method which might have its own limitations or advantages (Morais & de Almeida, 2012).

In this study, the group decision making was performed to collate the rankings provided by all the five used MCDM methods (i.e., CP, CGT, TOPSIS, WAT, and Fuzzy TOPSIS) over each grid into single representative ranks. Spearman rank correlation (Chowdhury et al., 2021) was used to find the average strength of each MCDM method (Srinivasa Raju & Nagesh Kumar, 2010) of each MCDM method. These average strengths were normalized using Norm-1 technique (eq. 3.1) for weight assignment to respective MCDM method for integrating the ranks.

3.2.5.1 Spearman rank correlation

The association between the ranks obtained using different MCDM methods can be assesed by Spearman rank correlation (ρ). If K_1 nd K_2 are the two different ranks of an alternative A_1 using two different approaches, then following Gibbons

& Chakraborti (2014), ρ can be expressed as,

$$\rho = 1 - \frac{6 \sum_{a=1}^{N} D_{A1}^2}{N\left(N^2 - 1\right)} \tag{3.15}$$

Where, D_{A1} is the difference between ranks i.e., $(K_1 - K_2)$, for the same alternative A_1, and N is the number of alternatives.

An example of average strength computation is presented in Table 3.6; ρ values ≤ 2 as and diagonal values are not considered in the computation as presented in the highlighted cell. Rank correlation classification provided by Connolly & Sluckin (1971) is presented in Table 3.7.

Table 3.6: Computation of average strength of each MCDM method using Spearman rank correlation coefficient

MCDM method	M1	M2	M3	M4	M5	Sum	Number of considered element	Average Strength
M1	⋱	0.94	0.88	0.31	0.48	2.61	4	0.65
M2	0.94	⋱	0.94	0.16	0.25	2.13	3	0.71
M3	0.88	0.94	⋱	0.19	0.73	2.55	3	0.85
M4	0.31	0.16	0.19	⋱	0.90	1.21	2	0.61
M5	0.48	0.25	0.73	0.90	⋱	2.36	4	0.59

(Average strength is estimated by dividing the sum of considered ρ values from number of considered elements.)

Table 3.7: Rank correlation classification

ρ value	Nature of relationship
0.9-1.0	Very strong
0.7-0.9	Marked
0.4-0.7	Substantial
0.2-0.4	Definite
≤ 0.2	Small (can be neglected)

3.2.5.2 Additive ranking rule

After computation of average strength of each MCDM method, the final representative rank of each alternative at each grid is computed using additive ranking rule (Srinivasa Raju & Nagesh Kumar, 2010) as follows,

$$R_A^M = \frac{\sum_{m=1}^{M} w_m K_A^m}{M} \tag{3.16}$$

Where, R_A^M is the final rank of each alternative after integrating all the ranks of that alternative obtained by M number of MCDM methods; w_m is the weight or relative influence of each MCDM method; and K_A^m is the rank obtained by each alternative using each MCDM method m.

Chapter 4

Results and Discussion

Based on the availability, length of temporal coverage and ease of access, global precipitation estimates (GPEs) from a total of five products namely, APHRODITE (1951-2015), PERSIANN-CDR (1983-2020), CHIRPS (1981-2019), CMORPH (1998-2020), IMERG (2000-2020) were selected for evaluation over western Himalayan Region 2.1. During the study, these products had temporal coverage of different length at the time of downloading from their respective web-portals or ftp servers. However, these products were evaluated for their skills in resolving regional climatology for the overlapping period of IMD grid product which is available from 1901-2020 at 0.25° spatial resolution. Except IMERG, which has a spatial resolution of 0.1°, all other afore-mentioned GPEs are available at 0.25° spatial resolution, though their grid system does not aligned with IMD grid system. Therefore, the IMERG data was aggregated at 0.25° spatial resolution and remapped at IMD gird system using Climate Data Operator (CDO) in Linux environment. Similarly, other products were also remapped at IMD grid system.

To evaluate the selected GPEs, IMD grids with raingauge stations were identified and subsequent analysis was carried out with reference to these grids. Skills of GPE in resolving the precipitation climatology of region vis-a-vis IMD gridded precipitation dataset was assessed using graphical method whereas the efficiency of GPEs in capturing light, moderate, and extreme events, defined by

threshold values (section 3.1), were studied using POD and FAR. Furthermore, the ranking of selected GPEs were perfromed employing the concepts of MCDM and GDM method as explained in Chapter 3.

4.1 Evaluation of GPEs in reproducing regional precipitation cycle

Regional precipitation cycle was compared with IMD precipitation for the complete length of records for respective GPEs (Figure 4.1 a,c,e,g, and i). For this mean monthly areal precipitation was computed for the WHR considering the monthly precipitation of all the selected grids. The comparative analysis was also performed for monthly areal precipitation across all the years to find the linear association between various GPEs and IMD precipitation (Figure 4.1 b,d,f,h, and j).

Precipitation from APHRODITE was evaluated for the highest length of records wherein a total of 65 years of data was used, followed by CHIRPS, PERSIANN-CDR, CMORPH, and IMERG for which 39, 37, 22 and 19 years of data were used, respectively. As depicted in Figure 4.1, IMERG reproduces the precipitation climatology with greater skill (Figure 4.1i) wherein it is found to follow the seasonal cycle of mean monthly regional precipitation as observed in IMD precipitation. Except IMERG, all other GPEs were observed to show underestimation in mean monthly regional precipitation. PERSIANN-CDR (Figure 4.1c) and CMORPH (Figure 4.1g) were found to show considerable underestimations in the monthly precipitation of Jan, Feb, Mar, Apr and May in pre-monsoon season and in Jul and Aug in the monsoon season. Likewise, CHIPRS (Figure 4.1e) show the considerable underestimation during Jan to May and in the month of Aug. However, APHRODITE, though, show underestimation in regional monthly precipitation, the considerable deviation is observed only in the month of Jul and Aug (Figure 4.1a) unlike PERSIANN-CDR, CHIRPS, and CMORPH.

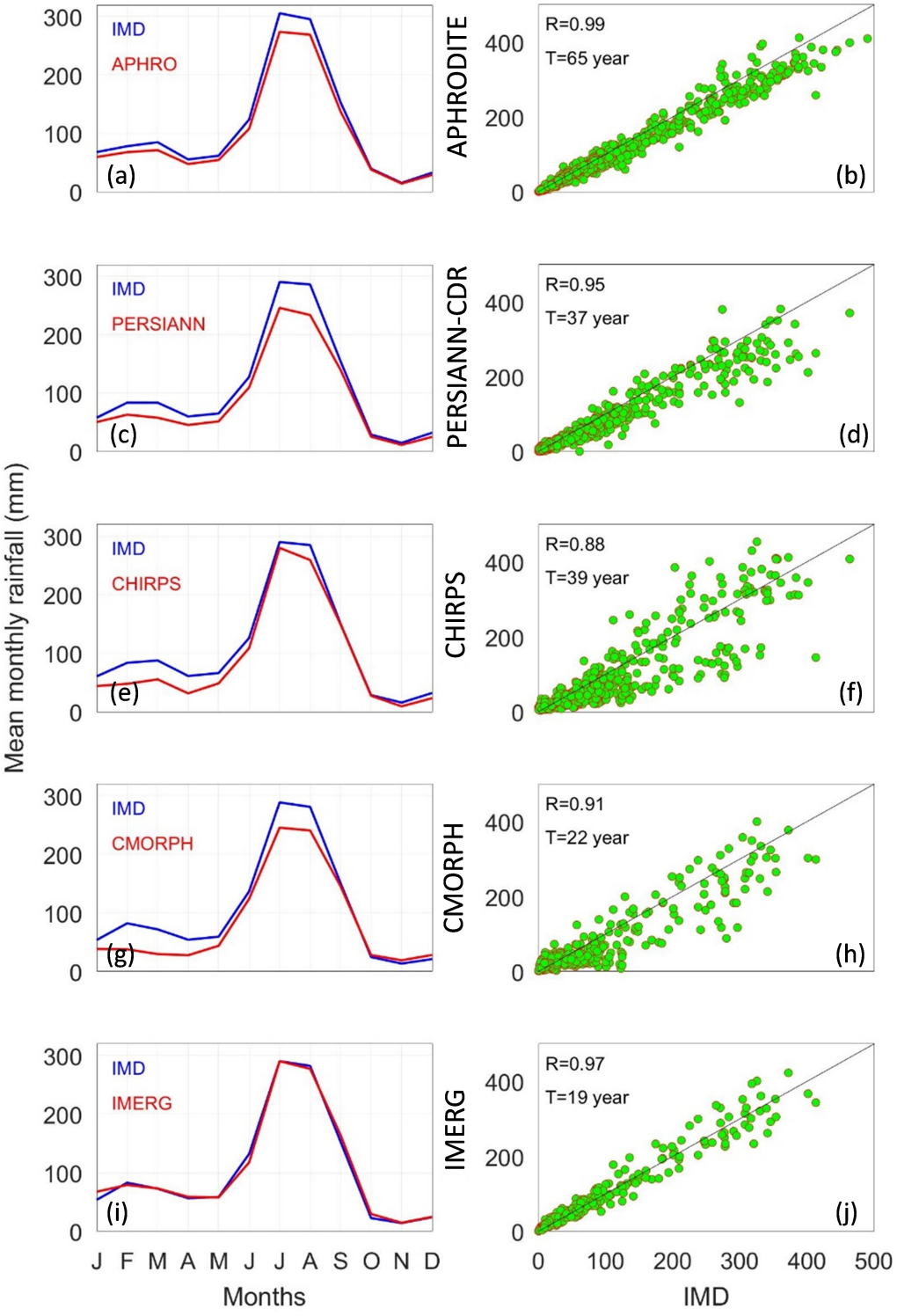

Figure 4.1: Comparison of regional precipitation of selected GPEs with IMD precipitation.

APHRODITE show the best performance, while comparing the year-wise monthly regional precipitation, wherein the Pearson correlation coefficient (denoted by R in the Figure 4.1) was found to be 0.99. However, for heavy events some under-estimation was observed (Figure 4.1b) which might have resulted in the under-estimation of monthly precipitation of Jul and Aug (Figure 4.1a). Good Pearson correlation was also observed in case of IMERG, however, both under-estimation and over-estimation in extreme events were observed (Figure 4.1j). Presence of both positive and negative deviation in the IMERG precipitation could be have balanced the error in the computation of mean monthly regional precipitation cycle (Figure 4.1i). PERSIANN-CDR (Figure 4.1d) and CMOPRH (Figure 4.1h) are found to be dominated by under-estimation of heavy events, wherein the CHIRPS showed both the under-estimation as well as over-estimation in the heavy events (Figure 4.1f) whereas the moderate events were found to be mostly under-reported like in CMORPH (Figure 4.1h).

4.2 Evaluation of GPEs in capturing light, moderate, and heavy events

Besides, evaluating the monthly precipitation across over regional scale, investigation was carried out to find the skills of selected GPEs in capturing the low, moderate and heavy precipitation defined using 50, 75, and 99 percentile threshold, respectively, as described in section 3.1.

4.2.1 Probability of Detection

It was found that, for heavy precipitation events all the GPEs show poor performance wherein POD was predominantly less than 0.2 for majority of grids (Figures 4.2f, i, l, and o) except APHRODITE (Figure 4.2c) wherein the POD values were also found to be distributed in the range of 0.2 to 0.4.

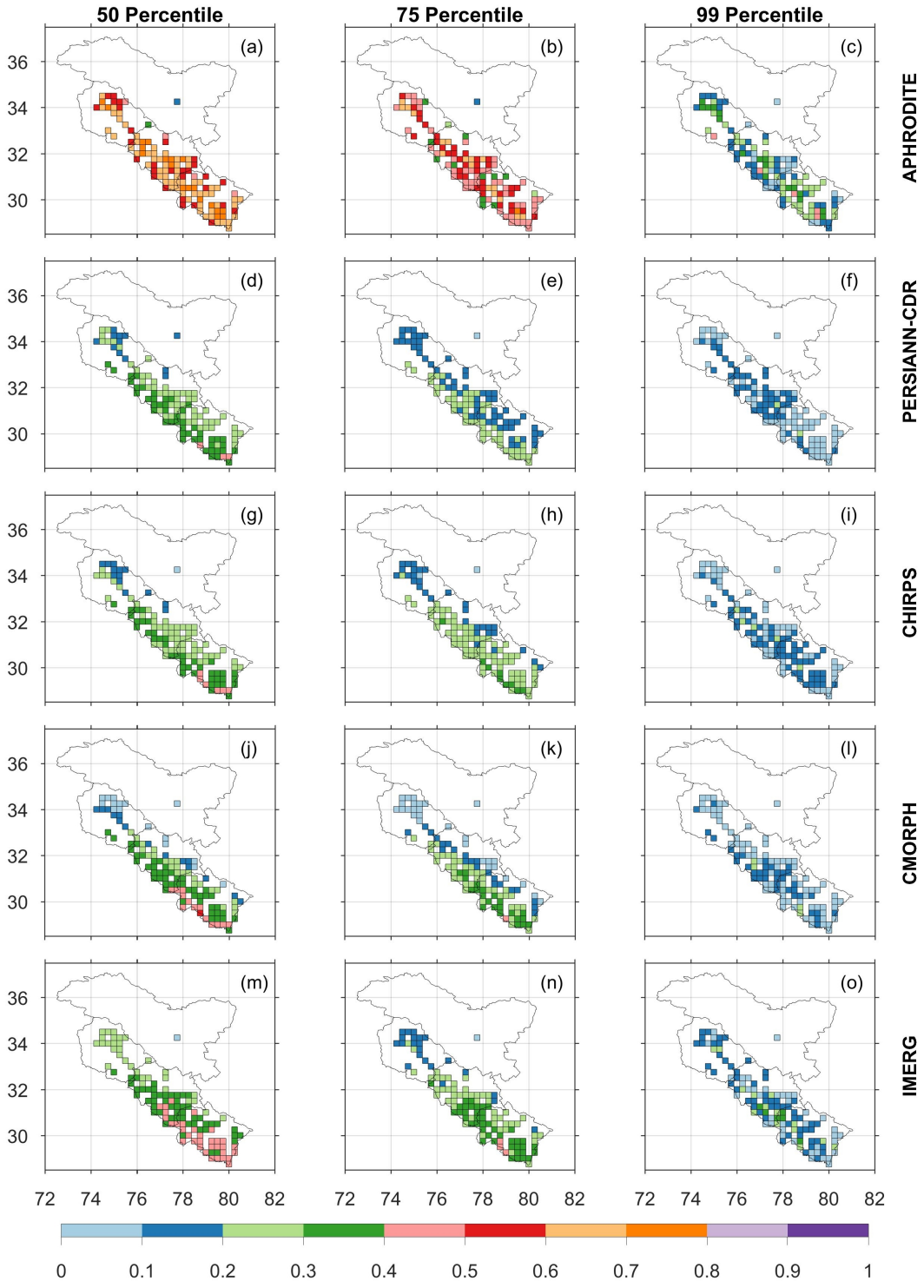

Figure 4.2: Spatial representation of POD for light (50 percentile), moderate (75 percentile) and heavy (99 percentile) precipitation threshold over identified grids across WHR.

Contrary, to heavy events, relatively improved POD values were observed in moderate and light precipitations events. Interestingly, the POD with smaller values were noticed for grids located in higher altitude regions (Figure 2.2) compared to relatively larger POD values in low altitude regions (Figures 4.2d, e, g, h, j, k, m, and n). It is worth noticing from the Figure 4.2 that for light precipitation events considerably higher POD values in comparison to PERSIANN-CDR (Figure 4.2d), CHIRPS (Figure 4.2g), CMORPH (Figure 4.2j) and IMERG (Figure 4.2m) were observed for APHRODITE (Figure 4.2a) wherein more than 60% of grids showed POD > 0.6.

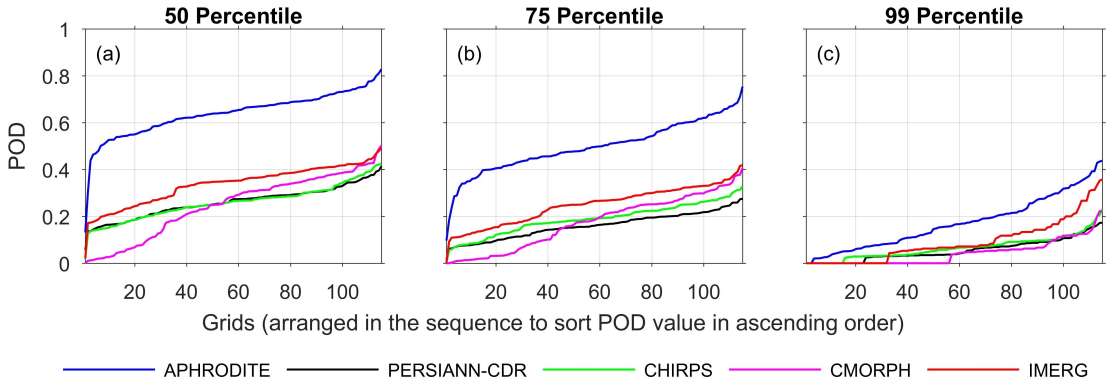

Figure 4.3: POD for light (50 percentile), moderate (75 percentile) and heavy (99 percentile) precipitation threshold over identified grids across WHR.

Form another Figure 4.3, which show the POD values for all the GPEs by the means of line plot, it can be clearly seen that for light and moderate precipitation events APHRODITE performs better than all other GPEs (Figures 4.3a and b). Here, it is worth to note that the POD values were arranged in ascending order for each GPE for ease of depiction of POD pattern and grid sequencing is likely to vary for different GPEs (i.e., POD = 0.3 can be read for different grids for different GPEs, and tick labels in x-axis in Figure 4.3 represent the grid counts only not the order or sequence). Though IMERG found to be performing better than other GPEs in capturing light (Figure 4.3a) and moderate (Figure 4.3b) events, it does not capture the events with acceptable accuracy. Likewise, for heavy precipitation events none of the GPE is found to produce POD > 0.5 (Figure 4.3c) which is also presented through spatial plots in Figure

4.2 for heavy precipitation events.

4.2.2 False Alarm Ratio

Unlike POD, smaller value is favourable in FAR. As shown in the spatial plots (Figure 4.4), high FAR in the range of 0.8 to 1.0 were observed for heavy precipitation events for PERSIANN-CDR (Figure 4.4f) , CHIRS (Figure 4.4i), CMORPH (Figure 4.4l), and IMERG (Figure 4.4o) which indicates poor performance of these GPEs. However, though not in the acceptable range, the APHRODITE is found to perform relatively better (Figure 4.4c).

The skills of GPEs studied using FAR are found to be similar as observed in POD analysis (section 4.2.1), wherein the APHRODITE performed comparatively better than other GPEs, in general, and showed higher skills for light and moderate precipitation events. As presented in Figures 4.4a and 4.4b, FAR is found to be within the range of 0.2 to 0.4 for majority of grids in case of APHRODITE for light and moderate events, respectively, which was otherwise found to be in higher range i.e., 0.6 to 0.7 for PERSIANN-CDR (Figures 4.4d and e), CHIRPS (Figures 4.4g and h), CMORPH (Figures 4.4i and j), and IMERG (Figures 4.4m and n).

Similar to the discussion made in section 4.2.1, besides presenting the spatial distribution of FAR in the region, FAR across all the grids were compared for all the GPEs for light, moderate, and heavy precipitation events (Figure 4.5). Evidently, APHRODITE shows the higher skills for light (Figure 4.5a) and moderate (Figure 4.5b) events wherein the FAR is found be within 0.2 to 0.4 for more than 65% of grids in the region. Also, higher error in heavy events can be seen in PERSIANN-CDR, CHIRPS, CMORPH, and IMERG (Figure 4.5c). Interestingly, though spatial pattern of FAR varies noticeably for PERSIANN-CDR (Figure 4.4d and e), CHIRPS (Figure 4.4g and h), CMORPH (Figure 4.4j and k), and IMERG (Figure 4.4m and n), these GPEs were found to have similar level of inaccuracies in their skills in case of light (Figure 4.5a) and moderate (Figure 4.5b) precipitation events.

4.2. Evaluation of GPEs in capturing light, moderate, and heavy events

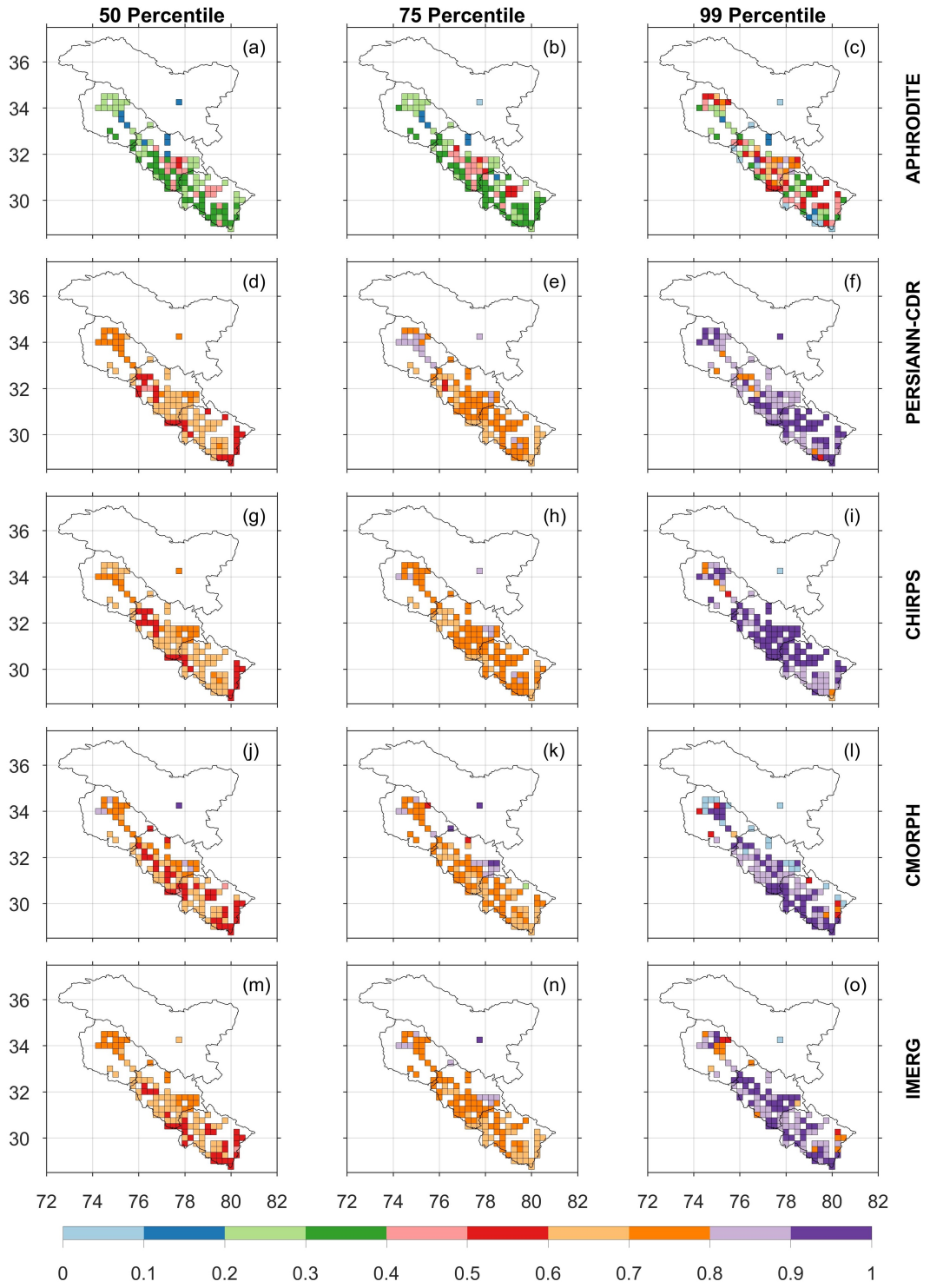

Figure 4.4: Spatial representation of FAR for light (50 percentile), moderate (75 percentile) and heavy (99 percentile) precipitation threshold over identified grids across WHR.

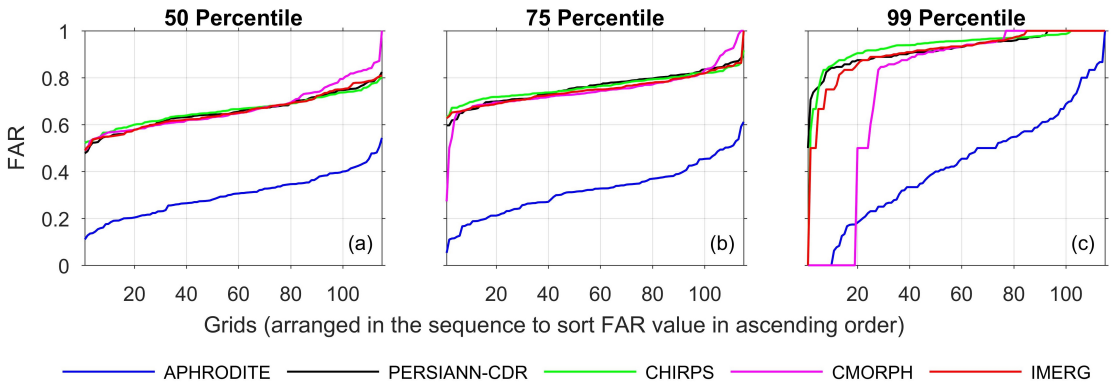

Figure 4.5: FAR for light (50 percentile), moderate (75 percentile) and heavy (99 percentile) precipitation threshold over identified grids across WHR.

4.3 Performance ranking of GPEs using MCDM methods

Grid-wise precipitation data for selected GPEs, i.e., APHRODITE, PERSIANN-CDR, CHIRPS, CMORPH, and IMERG were evaluated for their performance employing three performance indicators namely, NRMSE, CC, and SS (Table 3.1). However, it is worth to note that performance ranking was determined considering the data for common period, i.e.,01/Jan/2001 to 31/Dec/2015, during which precipitation is available for all the five GPEs. Common period is selected to avoid the ambiguity in final results that might arise due to varying period of dataset. As illustrated in Figure 3.1) and explained in section 3.2, a total of five different MCDM techniques i.e., CP, CGT, TOPSIS, WAT, and Fuzzy TOPSIS were employed to obtain the performance rank of each GPE for all the identified grids. Ranking of GPEs were obtained for daily time series (section 4.3.1), monthly time series (section 4.3.2), and monthwise time series (section 4.3.3) as discussed ahead.

4.3.1 MCDM based performance ranking using daily time series

Daily time series were employed to obtain the performance ranking for all the GPEs using different MCDM methods as explained in Chapter 3. Spatial map of performance indicators, i.e., NRMSD, CC, and SS for all the GPEs is presented in Figure 4.6. Smaller NRMSD and higher CC was observed for APHRODITE (Figures 4.6a and f), in comparison to PERSIANN-CDR (Figures 4.6b and g), CHIRPS (Figure 4.6c and h), CMOPRH (Figures 4.6d and i), and IMERG (Figures 4.6e and j) for a majority of grids. However, the skill-score (SS) is found to be in similar range in a majority of grids for APHRODITE (Figure 4.6k), CHIRPS (Figure 4.6m), CMORPH (Figure 4.6n), and IMERG (Figure 4.6o). Noticeably, PERSIANN-CDR performed 'comparatively' bad as revealed by relatively smaller SS values across the grids (Figure 4.6l).

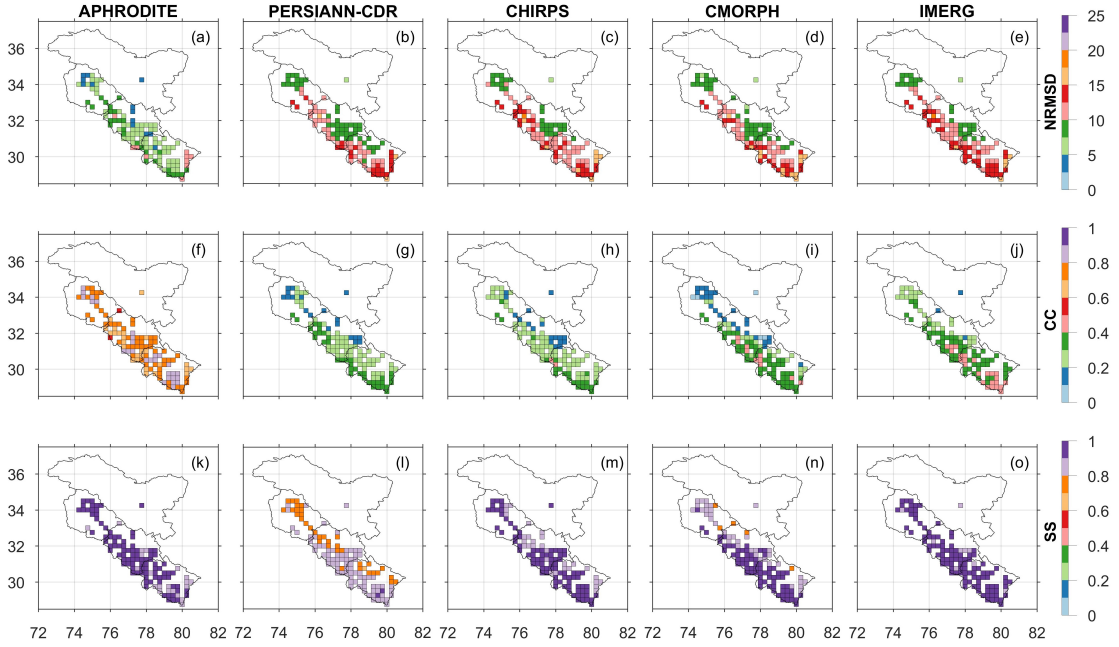

Figure 4.6: Spatial representation of performance indicator for daily time series.

As evident from the Figure 4.6, a varying range of performance indicators were obtained across different grids for different GPEs. Therefore, to suitably

utilize the strength and limitation of these performance indicators, their weights were determined using entropy technique for each grid as explained in section 3.2.2. As presented in Figure 4.7, NRMSD and SS show very high entropy values in the range $\in [0.9, 1)$, which infers that NRMSD and SS have large uncertainty associated with them. However, the CC showed lesser entropy in comparison to NRMSD and SS and in turn was assigned higher weight (eq. 3.4 and eq. 3.5) as shown in Figure 4.7. Also, NRMSD was assigned higher weights in comparison to SS, as it showed relatively smaller entropy.

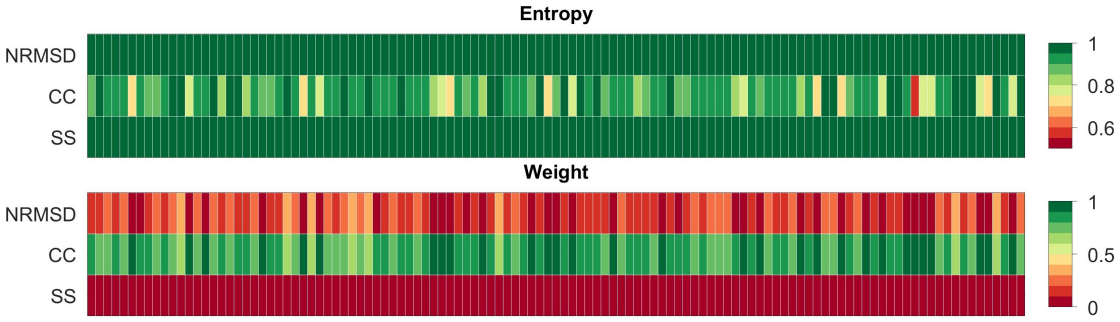

Note: *In x-axis, grids are sequentially arranged in same order, though not in any specific pattern, for all the figures.*

Figure 4.7: Entropy value and weight assigned to performance indicators for computing performance ranking employing daily time series.

Utilizing the weight obtained using entropy technique, performance ranking of GPEs were estimated for each grid as presented in Figure 4.8. It is evident from the Figure 4.8 that except APHRODITE, for all other GPEs, different ranks were assigned by different MCDM methods. Though form this figure APHRODITE can certainly be identified as best performing GPEs as all the GPEs ranked it 1 for al grids, except one instance where it was ranked 3 by CGT method, it is very difficult to assign any specific rank to other GPEs as different MCDM methods ranked them differently for considerable number of grids. Therefore, it is imperative to integrate the ranks obtained by different MCDM methods into a single representative rank employing GDM approach (as explained in section 3.2.5) which is presented in section 4.4.

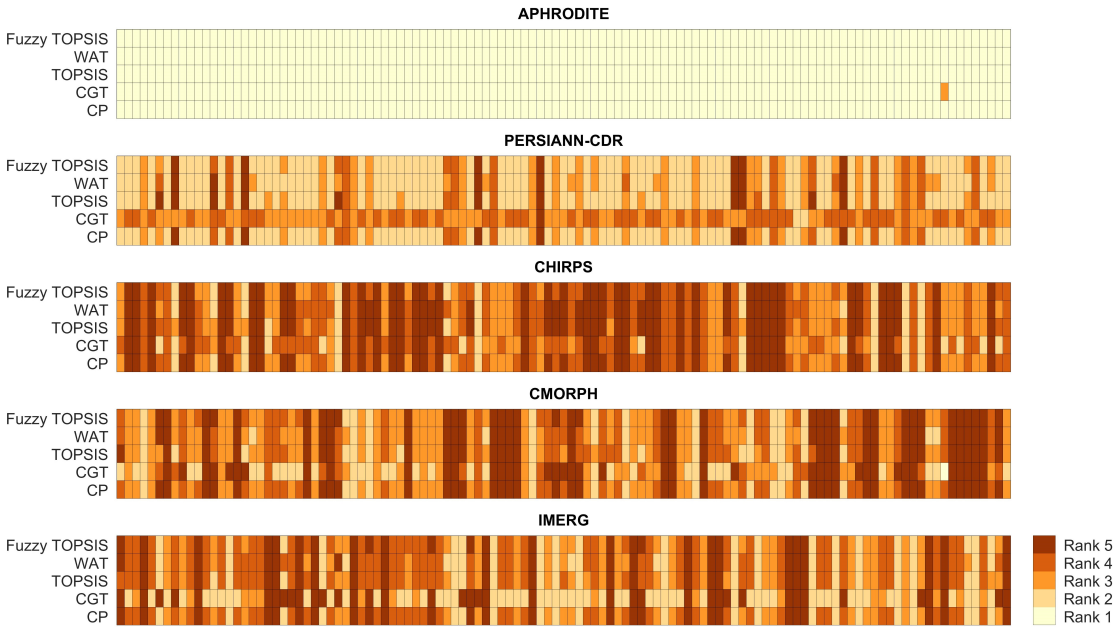

Note: *In x-axis, grids are sequentially arranged in same order, though not in any specific pattern, for all the figures.*

Figure 4.8: Performance ranking of GPEs employing daily time series and different MCDM techniques.

4.3.2 MCDM based performance ranking using monthly time series

For monthly time series, spatial representation of performance indicators is shown in Figure 4.9 for all the GPEs. Unlike daily time series, comparatively a well-mixed distribution of these indicators was noticed across the grids. Here it can be realized that in the absence of MCDM approach wherein all the different criterion can be integrated to assess the overall skill, it becomes very difficult to make any conclusive statement owing to the non-uniform variation of indicators across the grids. However, while comparing the monthly numbers with daily, it can be seen that skill score for all the GPEs has decreased for monthly time series (Figures 4.9k, l, m, m, and o) vis-a-vis daily time series (Figures 4.6k, l, m, m, and

o). Besides, the skill of APHRODITE as presented by NRMSD (Figures 4.9a-e) and CC (Figures 4.9f-j) is found to be less prominent in monthly time series in comparison to daily time series (Figures 4.6a-e and Figures 4.6f-j).

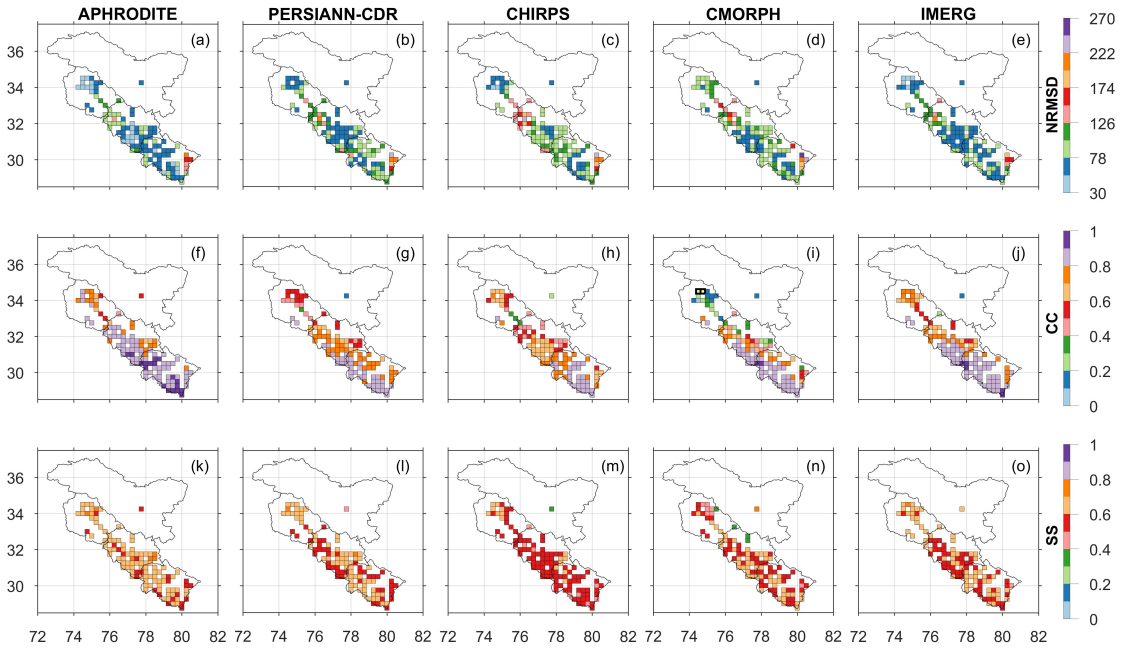

Figure 4.9: Spatial representation of performance indicator for monthly time series.

Though all the indicators show high entropy, unlike daily time series (Figure 4.7), weight distribution was found to changed considerably among NRMSD, CC, and SS (Figure 4.10) wherein the highest and lowest weights were also assigned to NRMSD and CC, respectively, for many of the grids. Utilizing these weights performance ranking of GPEs were estimated. For monthly time series, though APHRODITE was found to perform better than other GPEs in all the MCDM methods for a large majority of the grids (Figure 4.11), for few of the grids, multiple ranking were assigned to it as well as to other GPEs by different MCDM methods. In general, from Figure 4.11 it can be realized that the APHRODITE is followed by IMERG in terms of skill, it is difficult to make any inferences for other GPEs, i.e, PERSIANN-CDR, CHIRPS, and CMORPH. Therefore, to reach the conclusive statement GDM based rank integration is performed.

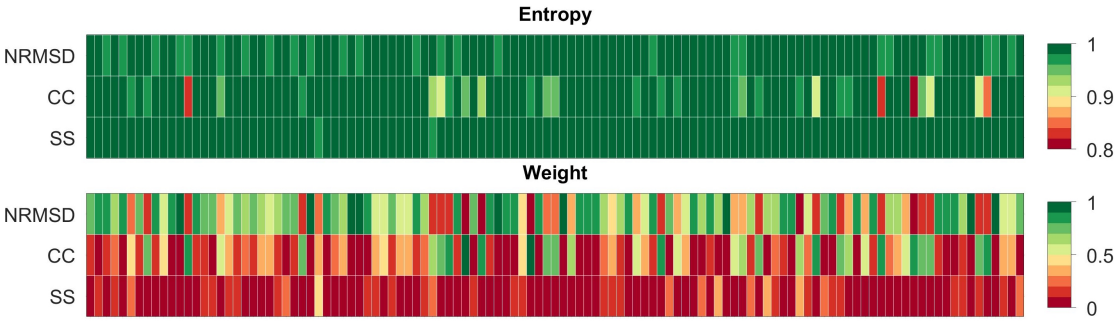

Note: *In x-axis, grids are sequentially arranged in same order, though not in any specific pattern, for all the figures.*

Figure 4.10: Entropy value and weight assigned to performance indicators for computing performance ranking employing monthly time series.

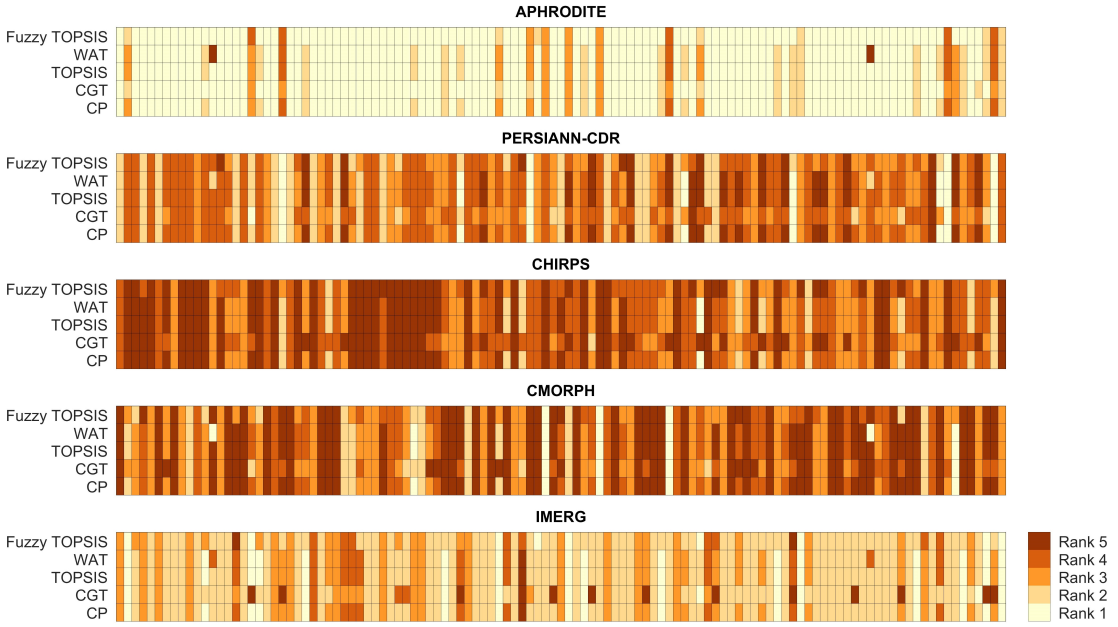

Note: *In x-axis, grids are sequentially arranged in same order, though not in any specific pattern, for all the figures.*

Figure 4.11: Performance ranking of GPEs employing monthly time series and different MCDM techniques.

4.3.3 MCDM based performance ranking using monthwise time series

After estimating the performance ranking of GPEs by analysing daily (section 4.3.1) and monthly time series (section 4.3.2), further analysis was performed for monthwise time series. In monthwise time series, daily data was arranged monthwise for each grid, and daily estimates of GPEs for specific months (e.g., July) was evaluated using the corresponding month of data from IMD product (i.e., July). In monthwise analysis, the entropy and weights were computed for each months for each grids (performance indicators not shown here) to apply in MCDM ranking methods. Contrary to daily time series SS showed higher entropy (Figure 4.7), in monthwise time series predominantly the SS showed 'relatively' lower entropy as shown in Figure 4.12.

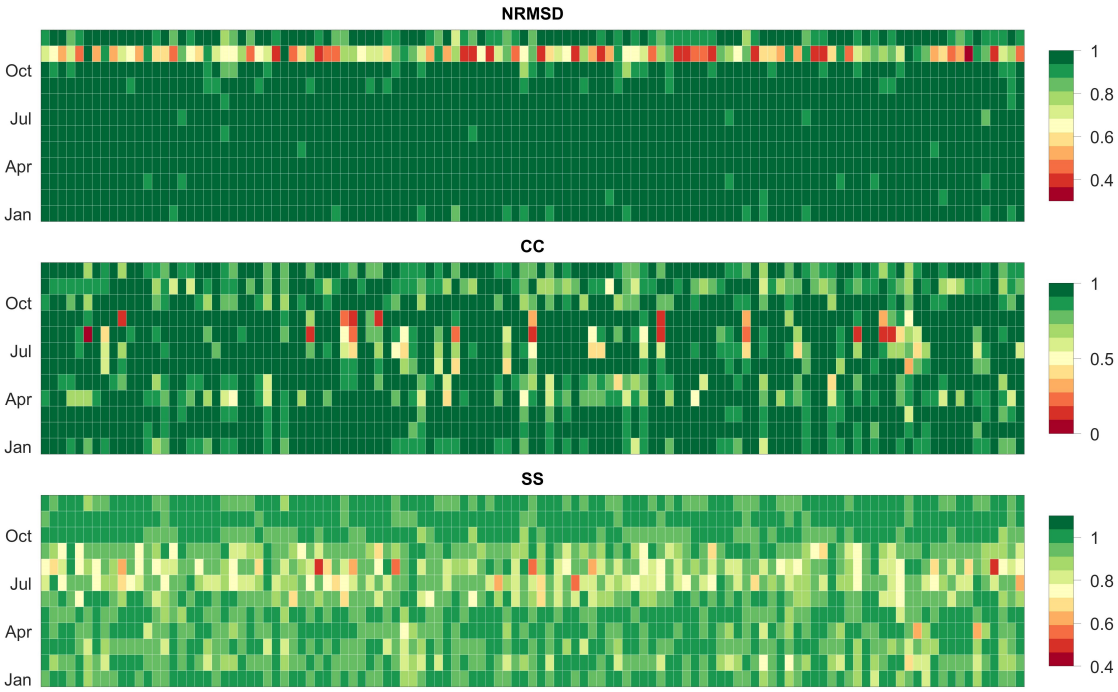

Note: *In x-axis, grids are sequentially arranged in same order, though not in any specific pattern, for all the figures.*

Figure 4.12: Entropy of performance indicators for computing performance ranking employing monthwise daily time series.

4.3. Performance ranking of GPEs using MCDM methods

After estimating the monthwise entropy for performance indicators in each grid, weight computation was performed for subsequent analysis. Weight distribution among NRMSD, CC, and SS across all the grid in different months of the year is presented in Figure 4.13.

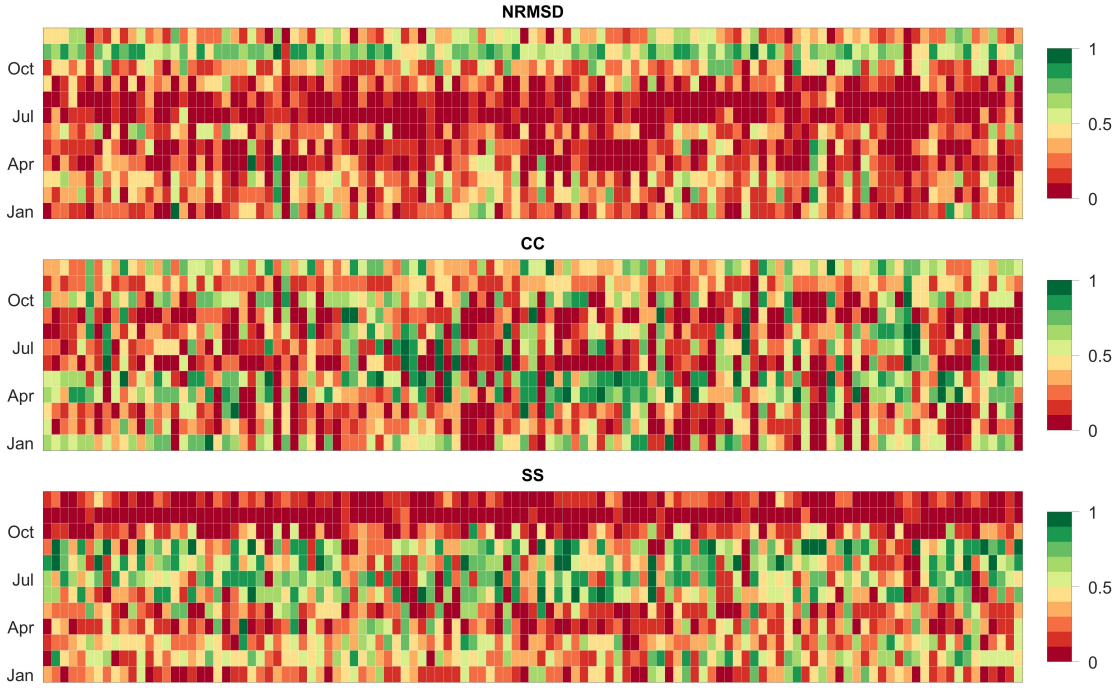

Note: *In x-axis, grids are sequentially arranged in same order, though not in any specific pattern, for all the figures.*

Figure 4.13: Weight assigned to performance indicators for computing performance ranking employing monthwise daily time series.

An Illustration for the month of July is provided herein for the obtained performance ranking of each GPE (Figure 4.14). Evidently, except few grids, different ranks were assigned to a particular GPE by different MCDM method. A wide range of variability in the GPE performance rank was found in multiple grid as estimated by different MCDM methods, therefore, to derive the conclusive results GDM based rank integration was performed.

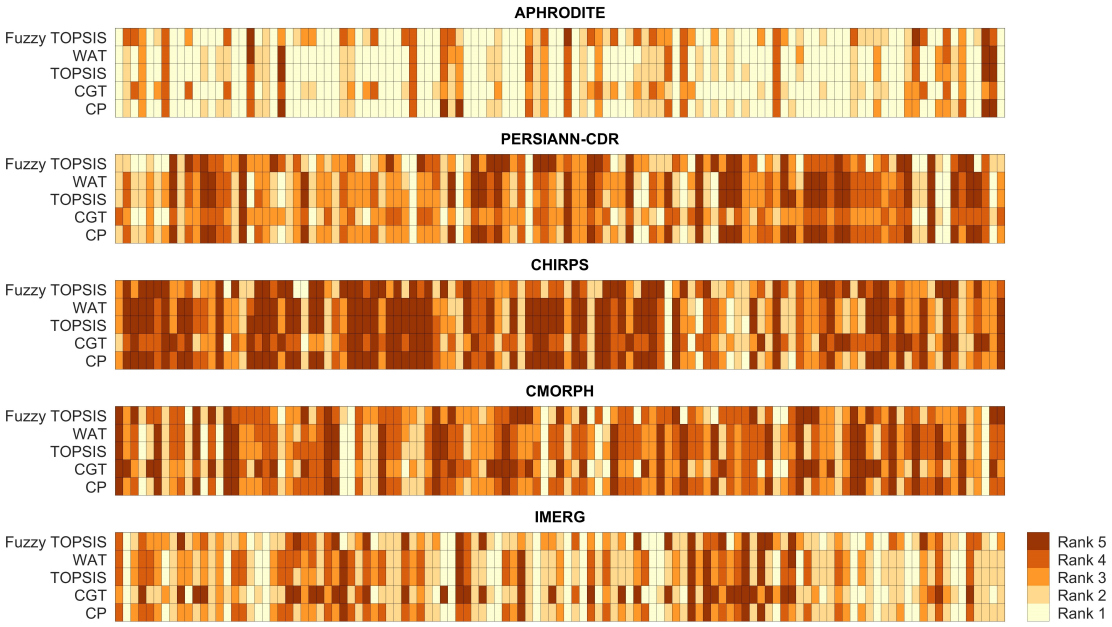

Note: *In x-axis, grids are sequentially arranged in same order, though not in any specific pattern, for all the figures.*

Figure 4.14: Performance ranking of GPEs employing monthwise time series and different MCDM techniques for the month of July.

4.4 Integration of performance ranking using GDM approach

As discussed in the previous sections, owing to the ambiguous results yielded by different MCDM methods for a specific GPE over a specific grid, it is imperative to integrate the results of different approaches to make a conclusive and informed decision. Therefore, the performance ranks of all the GPEs were integrated to derive a final rank utilizing the spearman correlation coefficient and additive ranking rule as explained in section 3.2.5.1 and section 3.2.5.2.

In following sections, gridwise integration of GPEs' ranks obtained using daily time series, monthly time series, and monthwise time series is presented.

4.4.1 Integration of performance ranking obtained using daily time series

For daily time series, APHRODITE is found to outrank all other GPEs wherein for all the grids it obtained rank 1 in GDM approach (Figures 4.15 and 4.16). However, for APHRODITE it was obvious as all the methods ranked it 1 in MCDM method (Figure 4.8). In other GPEs, i.e., PERSIANN-CDR, CHIRPS, CMORPH, and IMERG; PERSIANN-CDR was found to perform better than other GPEs for majority of the grids. Especially, PERSIANN-CDR is found to perform better in lower altitude region (Figure 4.15b) wherein for majority of the grids it was ranked second.

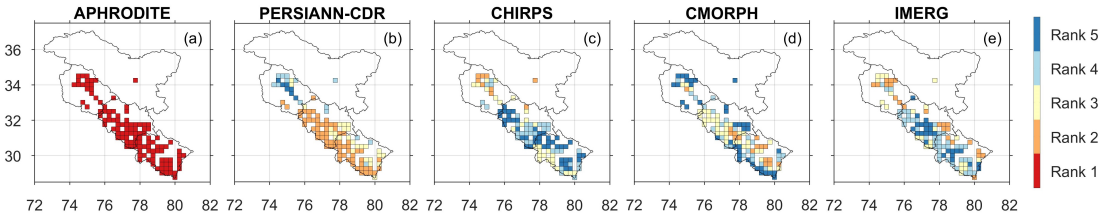

Figure 4.15: Spatial map of performance ranking of GPEs after applying GDM for daily time series.

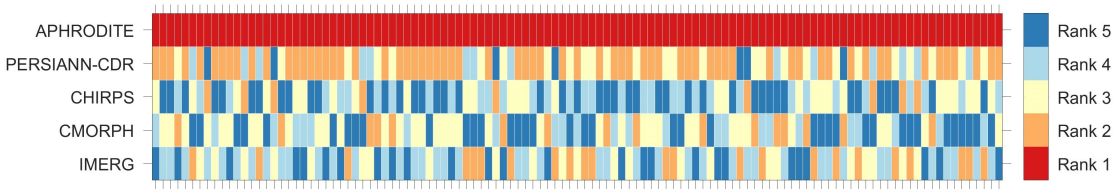

Note: *In x-axis, grids are sequentially arranged in same order, though not in any specific pattern, for all the figures.*

Figure 4.16: Color matrix of performance ranking of GPEs after applying GDM for daily time series.

PERSIANN-CDR was ranked after APHRODITE for maximum number of grids wherein a total of 67 grids it was assigned second rank (Table 4.1) with least number of grids showing last rank (i.e., rank 5). CHIRPS showed the poorest

Table 4.1: Grid counts versus GPEs' ranking for daily time series

	Rank 1	Rank 2	Rank 3	Rank 4	Rank 5
APHRODITE	115	0	0	0	0
PERSIANN-CDR	0	67	27	14	7
CHIRPS	0	9	28	34	44
CMORPH	0	16	37	24	38
IMERG	0	23	23	43	26

performance wherein for maximum number of grids it was assigned last rank and for only 9 grids it was ranked second.

4.4.2 Integration of performance ranking obtained using monthly time series

For monthly precipitation time series, APHRODITE was found to perform better across the region wherein it was assigned first rank (Figures 4.17 and 4.23). Interestingly, PERSIANN-CDR which performed comparatively better while ranking the GPEs for daily time series, found to have deterioration in its ranking for monthly time series as many of the grids were assigned second and third rank (Figure 4.17b) after IMERG (Figure 4.17e).

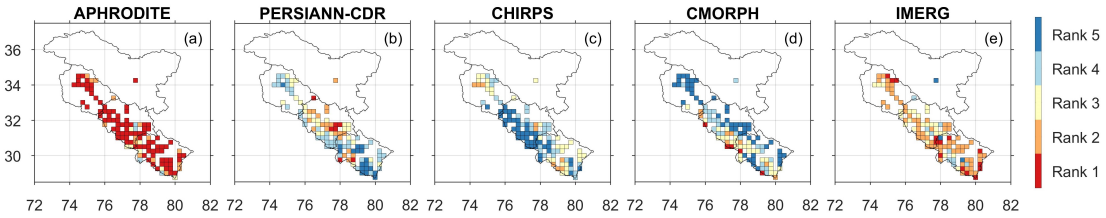

Figure 4.17: Spatial map of performance ranking of GPEs after applying GDM for monthly time series.

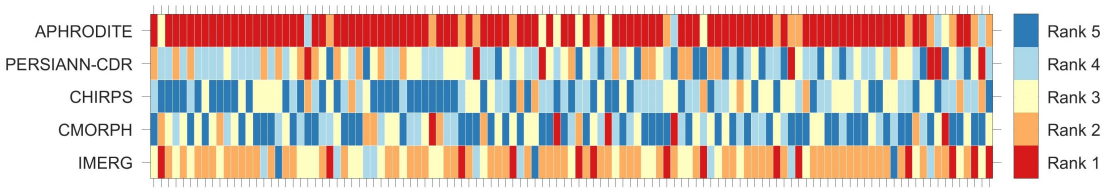

Note: *In x-axis, grids are sequentially arranged in same order, though not in any specific pattern, for all the figures.*

Figure 4.18: Color matrix of performance ranking of GPEs after applying GDM for monthly time series.

APHRODITE was assigned first rank in a total of 89 number of grids, followed by IMERG which was ranked 1 in only 14 number of grids (Table 4.2). IMERG was found to perform better than other GPEs as it was assigned second rank for a total of 63 number of grids whereas in only 3 grids it was ranked last. Among all the GPEs, CHIRPS and CMOPRH were found to have poor performance as they were assigned last rank for most number of grids, i.e., 44 and 50, respectively. Noticeably, for none of the grids APHRODITE was assigned last rank contrary to CHIRPS which was not ranked first in any of the grids.

Table 4.2: Grid counts versus GPEs' ranking for monthly time series

	Rank 1	Rank 2	Rank 3	Rank 4	Rank 5
APHRODITE	89	15	7	4	0
PERSIANN-CDR	7	20	26	44	18
CHIRPS	0	9	29	33	44
CMORPH	5	8	27	25	50
IMERG	14	63	26	9	3

4.4.3 Integration of performance ranking obtained using monthwise time series

Similar to the GPE's rank integration using GDM approach in daily and monthly time series, GPE's rank for different months were also integrated to derive meaningful inferences. Spatial representation of GPEs' rank distribution across different grids in the WHR for different months is presented in Figures 4.19, 4.20, 4.21, and 4.22. Though spatial map helps in visualizing the distribution across space, a more concise and comprehensible information can be shown with the color matrix plot (Figure 4.23). Evidently, for majority of the grids APHRODITE was assigned top ranks for across all the months, followed by IMERG (Figure 4.23, Table 4.3). Performance of GPEs were found to be changing wherein number of grids with specific performance ranking of GPE is markedly changed in different months of the year. For example, APHRODITE was assigned first rank in 94 grids for the month of November which reduced to 61 grids in August (Table 4.3). Similarly, PERSIANN-CDR which was ranked second in 16 number of grids in August was not assigned second rank in any of the grid in November. On the contrary, it showed maximum deterioration wherein it was ranked last in a total of 96 grids in November compared to 21 grids in August. Noticeably, for these two months IMERG ranked after APHRODITE for majority of the grids and for few grids it even outranked APHRODITE. Here it is worth to note that Chowdhury et al. (2021) evaluated different satellite and reanalysis precipitation products including IMD gridded precipitation with station data for Satluj river basin for eight location. They reported APHRODITE as the best suitable product after IMD gridded precipitation based on the similar performance ranking exercise involving MCDM and GDM approaches.

It can be seen in Figure 4.23 that PERSIANN-CDR is ranked 4 and 5 for a majority of grids for the months of November and December which is in contrast to its performance for other months of the year. Similarly from the Figure 4.23, inferences about poor performance of CHIRPS and CMORPH can be drawn as they were ranked either 4 or 5 for majority of grids. A detailed information regarding grid counts of GPEs' rank for more insight can be referred in Table 4.3.

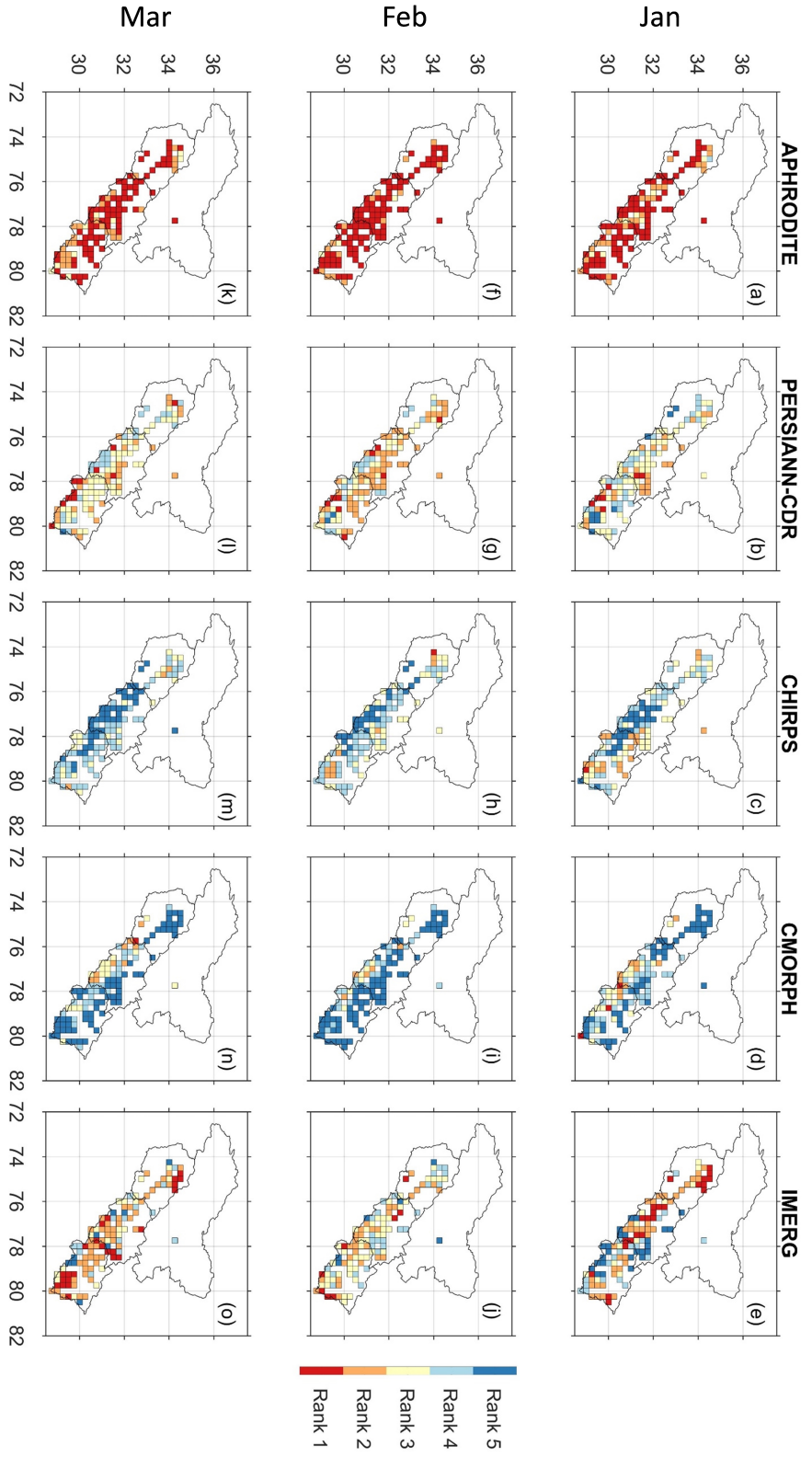

Figure 4.19: Spatial map of performance ranking of GPEs for Jan-Feb-Mar after applying GDM for monthwise daily time series.

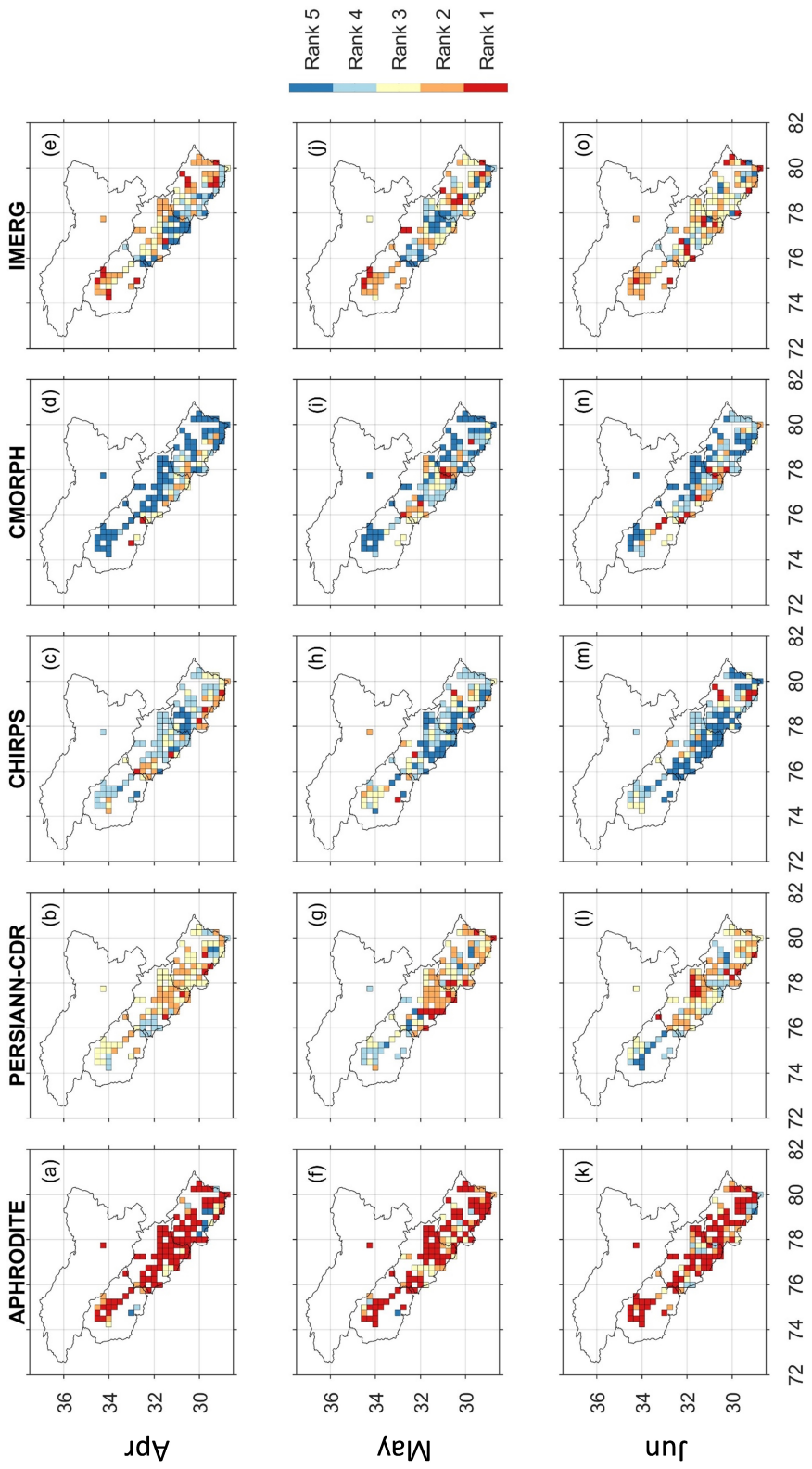

Figure 4.20: Spatial map of performance ranking of GPEs for Apr-May-Jun after applying GDM for monthwise daily time series.

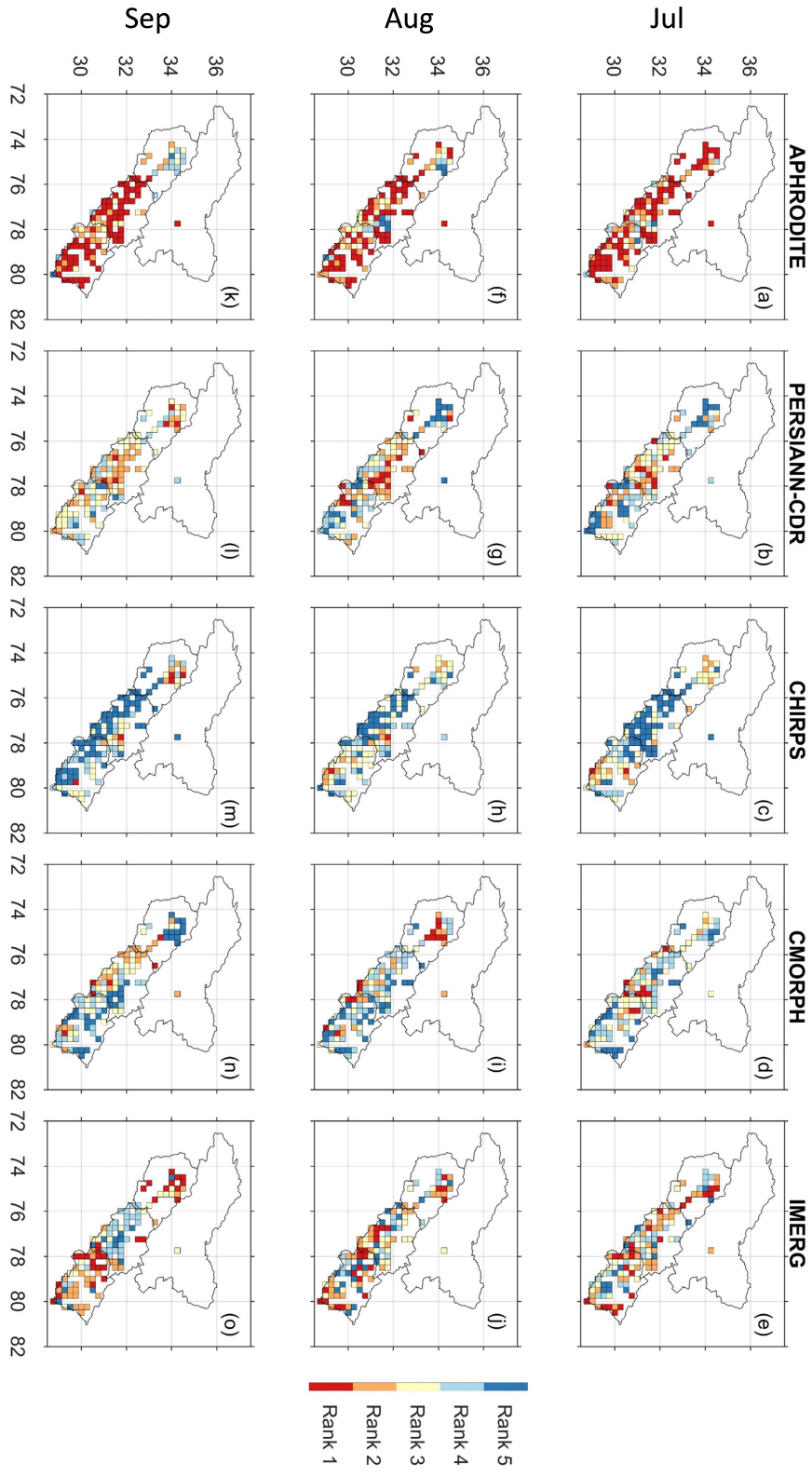

Figure 4.21: Spatial map of performance ranking of GPEs for Jul-Aug-Sep after applying GDM for monthwise daily time series.

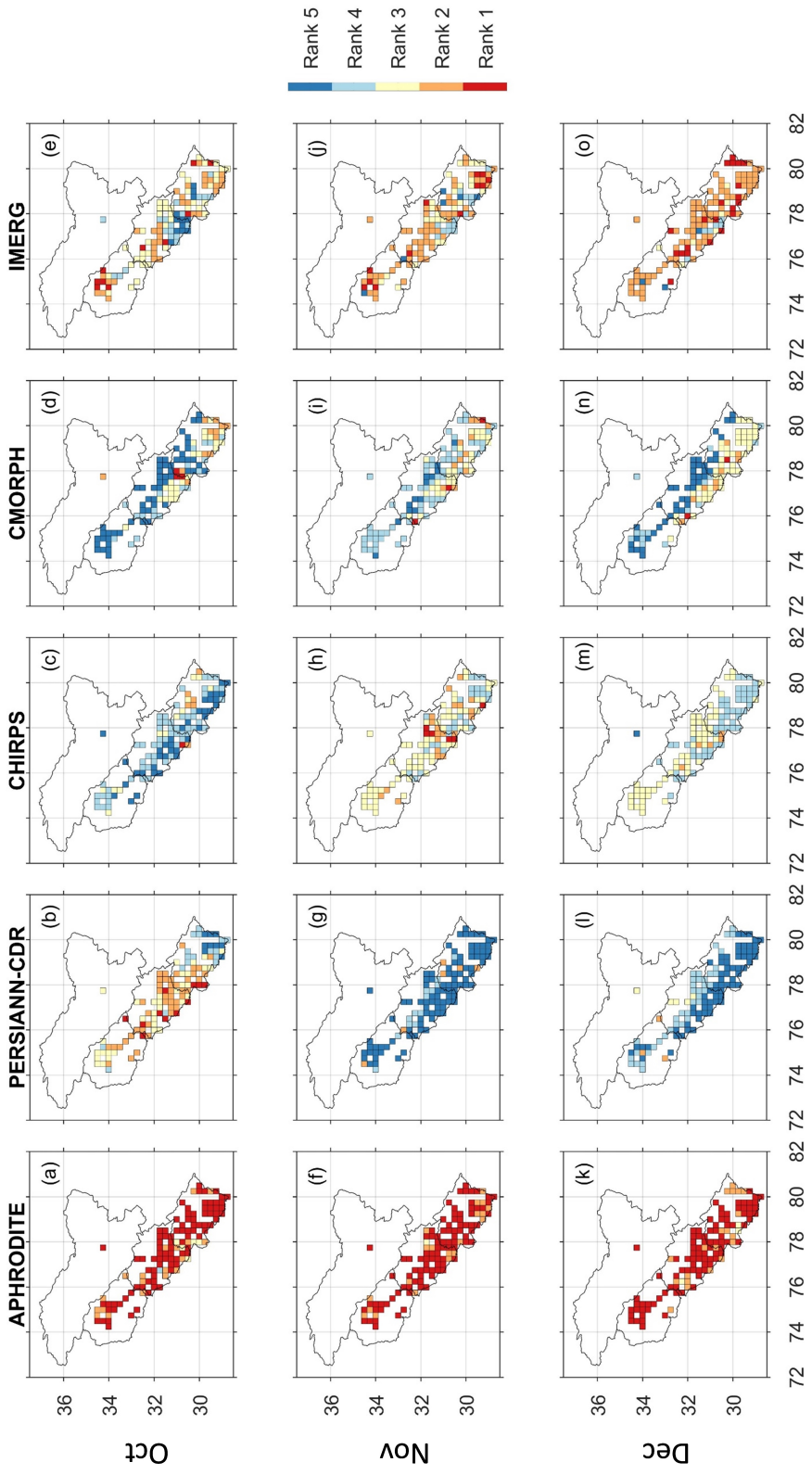

Figure 4.22: Spatial map of performance ranking of GPEs for Oct-Nov-Dec after applying GDM for monthwise daily time series.

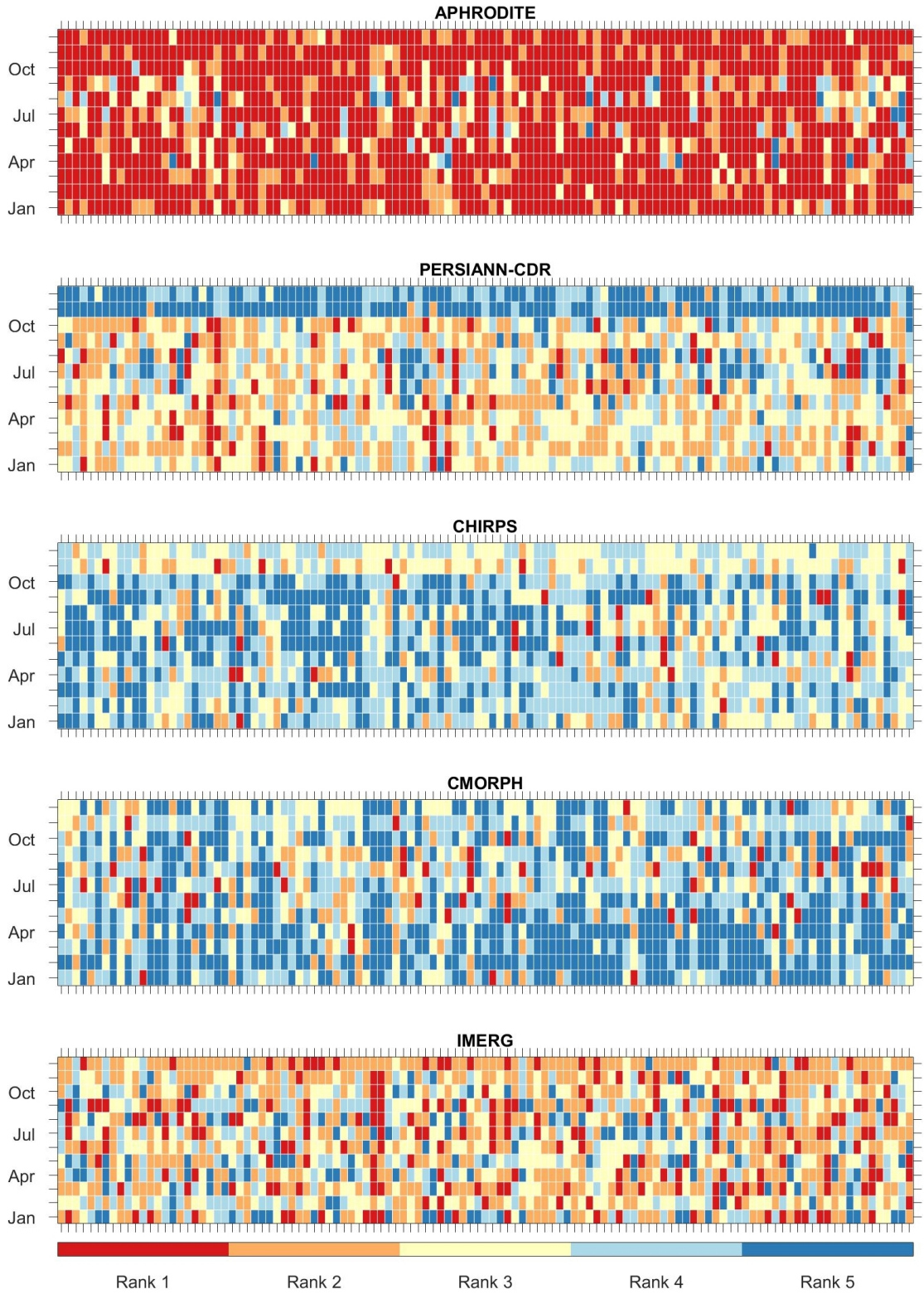

Figure 4.23: Color matrix of performance ranking of GPEs for each month after applying GDM for monthwise daily time series.

Table 4.3: Grid counts versus GPEs' ranking for monthwise daily time series

		Rank 1	Rank 2	Rank 3	Rank 4	Rank 5
Jan	**APHRODITE**	81	26	7	1	0
	PERSIANN-CDR	7	24	48	27	9
	CHIRPS	1	19	31	36	28
	CMORPH	3	10	17	32	53
	IMERG	23	36	12	19	25
Feb	**APHRODITE**	97	15	3	0	0
	PERSIANN-CDR	9	56	30	18	2
	CHIRPS	1	9	29	49	27
	CMORPH	0	5	8	22	80
	IMERG	8	30	45	26	6
Mar	**APHRODITE**	79	27	9	0	0
	PERSIANN-CDR	11	27	52	24	1
	CHIRPS	0	3	20	51	41
	CMORPH	1	9	15	26	64
	IMERG	24	49	19	14	9
Apr	**APHRODITE**	89	9	8	3	6
	PERSIANN-CDR	5	38	52	18	2
	CHIRPS	5	18	19	59	14
	CMORPH	2	10	15	15	73
	IMERG	14	40	21	20	20
May	**APHRODITE**	79	16	16	3	1
	PERSIANN-CDR	14	43	29	21	8
	CHIRPS	4	10	26	39	36
	CMORPH	6	14	16	31	48
	IMERG	12	32	28	21	22

Jun	**APHRODITE**	75	21	8	10	1
	PERSIANN-CDR	11	35	37	23	9
	CHIRPS	6	6	16	33	54
	CMORPH	8	14	13	37	43
	IMERG	15	39	41	12	8
Jul	**APHRODITE**	72	26	7	8	2
	PERSIANN-CDR	10	27	28	25	25
	CHIRPS	2	15	32	14	52
	CMORPH	9	12	30	42	22
	IMERG	22	35	18	26	14
Aug	**APHRODITE**	61	22	17	7	8
	PERSIANN-CDR	16	30	21	27	21
	CHIRPS	2	13	40	21	39
	CMORPH	13	18	14	44	26
	IMERG	23	32	23	16	21
Sep	**APHRODITE**	68	20	13	12	2
	PERSIANN-CDR	7	38	40	25	5
	CHIRPS	5	7	20	24	59
	CMORPH	6	21	25	27	36
	IMERG	29	29	17	27	13
Oct	**APHRODITE**	90	19	5	1	0
	PERSIANN-CDR	11	44	34	17	9
	CHIRPS	1	6	12	59	37
	CMORPH	3	12	24	19	57
	IMERG	10	34	40	19	12

Nov	**APHRODITE**	94	20	1	0	0
	PERSIANN-CDR	0	6	0	13	96
	CHIRPS	6	20	62	27	0
	CMORPH	3	11	27	61	13
	IMERG	12	58	25	14	6
Dec	**APHRODITE**	92	20	3	0	0
	PERSIANN-CDR	0	3	5	40	67
	CHIRPS	0	5	55	54	1
	CMORPH	2	9	45	15	44
	IMERG	21	78	7	6	3

From the discussion made in sections 4.4.1, 4.4.2, and 4.4.3, it can be seen that results of different MCDM techniques can be collated to obtain into single outcome using GDM approaches. It was found that though for majority of the grids APHRODITE outranked other GPEs while evaluating for monthly time series (Table 4.2) and monthwise time series (Table 4.3), for many grids other GPEs found to perform better. This could play an important role when the hydrological analysis is targeting the grid based response, as the wrongful omission of best performing GPE might result in misleading outcomes. On the contrary, over a basin scale that may include multiple grid the APHRODITE can be used; however, it is worth to explore how different GPEs contribute to the performance of final results of hydrological analysis, say, river discharge simulation in hydrological modeling. Besides, the performance ranking obtained in MCDM methods used IMD gridded product as the reference data, therefore, the accuracy of IMD gridded product or station data used in creating the IMD gridded product play a vital role on the overall outcome of the performance ranking. In an ideal approach the GPEs should be evaluated utilizing station data, however, it often becomes difficult and time consuming to collect station data for a vast region such as WHR and perform quality control and gap filling.

Chapter 5

Summary and Conclusions

5.1 Overview

Precipitation is one of the prime inputs in any hydrological analysis which strives for water resources management of any region. Western Himalayan Region (WHR) is an important region not only for strategic point of view but also for water resources as many rivers viz., Ganga, Yamuna, Satluj, Beas, Ravi, Chenab, Jhelum, etc. originates from this region. Owing to the changing hydrologic regime across the globe it is essential to study the response of these rivers with respect to climate change and develop decision support system to better manage the water resources. However, due to sparse network of raingauge network in the Himalayan region, which can be attributed to complex terrain and harsh climate, it becomes very difficult to obtain good quality precipitation data for analysing the changing status of river regime. Limitation caused be poor ground network can be tackled to a great extent by utilizing the satellite data or global precipitation estimates (GPEs) which have been made available to hydrologist by many agencies and organizations across the globe. In recent decades, range of global precipitation products have been released which can be employed for hydrological analysis, however, prior to their application to specific area it is advisable to evaluate them with respect to the study area.

Keeping above discussion in view, following specific objectives were formulated for this study,

1. Spatial and temporal aggregation of various global precipitation estimates to compare with IMD gridded precipitation product.

2. Statistical evaluation of global precipitation estimates to assess their skills in resolving regional precipitation climatology and extreme events .

3. Identification of suitable GPEs through performance ranking for WHR employing Multicriterion Decision Making and Group Decision Making approaches.

As aforesaid, the aim of this research was to evaluate various GPEs for their skills in resolving regional precipitation climatology of WHR. For this a total of five GPEs, namely, APHRODITE, PERSIANN-CDR, CHIRPS, CMORPH, and IMERG were selected based on the ease of accessibility and length of availability at the time of this study (Table 2.1). These GPEs were evaluated against IMD gridded precipitation product for their skills in reproducing the regional precipitation climatology with respect to IMD data and ability to capture light, moderate, and heavy precipitation defined by 50, 75, and 99 percentile threshold, respectively.

Selected GPEs were evaluated for daily, monthly, and monthwise precipitation time series for all the grids. Probability of detection (POD) and False Alarm Ratio (FAR) were used to evaluate the GPEs' skills for light, moderate, and heavy precipitation events across all the grids (section 4.2) whereas the precipitation climatology was studied using graphical method (section 4.1). Multicriterion Decision Making (MCDM) approaches (section 4.3 which utilizes Compromise Programming (section 3.2.3.1), Cooperative Game Theory (section 3.2.3.2), TOPSIS (section 3.2.3.3), Weighted Average Technique (section 3.2.3.4), and Fuzzy TOPSIS (section 3.2.4.1) were used for estimating the performance ranking of each GPE across all the grids. Performance indicators (section 3.1) i.e., Normalized Root Mean Square Deviation (NRMSD), Pearson Correlation Coefficient (CC),

and Skill Score (SS) were utilized in all the MCDM techniques wherein the entropy based weight assignment (section 3.2.2) to these indicators were performed for rank estimation. The performance rankings of each GPE obtained using different MCMD method then integrated employing Group Decision Making (GDM) technique (section 4.4) which uses spearman correlation coefficient (section 3.2.5.1) and additive ranking rule (section 3.2.5.2).

5.2 Conclusions

Based on the analysis carried out following specific conclusion were derived,

1. IMERG and APHRODITE reproduce the regional precipitation cycle with greater skill as compared to PERSIANN-CDR, CHIRPS, and CMORPH when analyzed for their entire length of data.

2. CMORPH underestimate the regional monthly precipitation across all the values more than the instances of over-estimation.

3. Both under- and over-estimation in the regional monthly precipitation was found in the case of CHIRPS.

4. PERSIANN-CDR predominately under-estimates the regional monthly precipitation.

5. None of the GPEs found to perform with agreeable accuracy for the heavy precipitation events, defined by 99 percentile threshold, as revealed by smaller POD and higher FAR.

6. APHRODITE is found to perform comparatively better than other GPEs for the light and moderate precipitation events defined by 50 and 75 percentile threshold, respectively as revealed by higher POD and smaller FAR for a majority of the grids.

7. Different MCDM methods were found to assign different performance ranks to specific GPEs in a same grid which can be attribute to the difference in their rank computation approach.

8. For daily precipitation, APHRODITE was found to outrank all other GPEs.

9. For monthly precipitation, Followed by IMERG, APHRODITE was found to outrank all the GPEs in majority of the grids.

10. For monthwise daily precipitation, APHRODITE was found to perform better for majority of the grids across all the months.

11. GPEs were found to outrank each other interchangeably for different month in many of the grids in monthwise daily precipitation.

12. CHIRPS and CMOPRH were found to be least favourable GPEs for majority of the grids.

5.3 Challenges and limitations of the study

The study utilizes the IMD gridded precipitation product for performing the evaluation and ranking of selected GPEs. However, as IMD gridded precipitation product itself is developed using station precipitation records, it is also expected to be affected by the limitation of station network in the mountainous terrain of WHR. Also, as it is understood that precipitation variability over space would be more in the mountainous region than the plains, it is likely that limited numbers of station available within a grid may not represent the grid rainfall completely. Despite this limitation IMD gridded product developed from station data has been widely used as benchmark data in numerous studies. However, a more improved approach could be usage of station records to perform the evaluation and ranking of GPEs which could not be done in this study. Here, it is to be noted that it is quite difficult to obtain long-term station record for each grid due to unavailability or non-functioning of the station itself.

5.4 Contributions and recommendations for future work

The work carried out in this study not only has many practical and scientific implications but also the findings of the study would be immensely helpful hydrologists in studying the water resources or river basin response under the influence of climate change in WHR. The two major contributions of the study include:

1. Though there are numerous studies evaluating the global precipitations across India or specific regions of WHR, none of the studies has categorically performed the GPE ranking on such scale.
2. Application of Multicriterion Decision Making approaches utilize the skills of different performance indicators in ranking the product, whereas the Group Decision Making technique integrates the different ranks by assigning suitable weights to each MCDM approach. The methodology adopted in this study ensure the robust and reliable outcomes which can be used by the researchers and water managers with greater confidence.

Addressal of limitation and challenges faced in this research work can be considered in further fine-tuning the results and bringing more insight into the findings. Below are the four recommendations which can be taken up in future research:

1. Availability of ground based precipitation records from various agencies can be explored to evaluate the GPEs with station data, instead of IMD gridded products.
2. More number of performance indicators can be employed in MCDM methods to rank different GPEs.
3. Different reanalysis products (e.g., ERA5, IMDAA, MERRA, CFSR, etc.) and other GPEs (e.g., SM2RAIN, MSWEP, GSMaP, etc.) can be included to further extend the analysis.

4. Different GPEs, after being ranked using MCDM and GDM approach, can be employed in hydrological modelling to study their rank using simulated response.

References

Andermann, C., Bonnet, S., & Gloaguen, R. (2011). Evaluation of precipitation data sets along the himalayan front. *Geochemistry, Geophysics, Geosystems*, *12*(7).

Arora, M., Singh, P., Goel, N., & Singh, R. (2006). Spatial distribution and seasonal variability of rainfall in a mountainous basin in the himalayan region. *Water Resources Management*, *20*(4), 489–508.

Azadi, M., Mohanty, U., Madan, O., & Padmanabhamurty, B. (2002). Prediction of precipitation associated with a western disturbance using a high-resolution regional model: role of parameterisation of physical processes. *Meteorological Applications*, *9*(3), 317–326.

Banerjee, A., Dimri, A., & Kumar, K. (2020). Rainfall over the himalayan foot-hill region: present and future. *Journal of Earth System Science*, *129*(1), 1–16.

Basistha, A., Arya, D., & Goel, N. (2008). Spatial distribution of rainfall in indian himalayas–a case study of uttarakhand region. *Water Resources Management*, *22*(10), 1325–1346.

Basistha, A., Arya, D., & Goel, N. (2009). Analysis of historical changes in rainfall in the indian himalayas. *International Journal of Climatology: A Journal of the Royal Meteorological Society*, *29*(4), 555–572.

Beria, H., Nanda, T., Singh Bisht, D., & Chatterjee, C. (2017). Does the gpm mission improve the systematic error component in satellite rainfall estimates over trmm? an evaluation at a pan-india scale. *Hydrology and Earth System Sciences*, *21*(12), 6117–6134.

Bhadwal, S., Ghosh, S., Gorti, G., Govindan, M., Mohan, D., Singh, P., Singh, S., & Yogya, Y. (2017). The upper ganga basin: Will drying springs and rising floods affect agriculture? *HI-AWARE working paper*, *8*.

Bharti, V., Singh, C., Ettema, J., & Turkington, T. (2016). Spatiotemporal characteristics of extreme rainfall events over the northwest himalaya using satellite data. *International Journal of Climatology*, *36*(12), 3949–3962.

Bhatt, B. C., & Nakamura, K. (2005). Characteristics of Monsoon Rainfall around the Himalayas Revealed by TRMM Precipitation Radar. *Monthly Weather Review*, *133*(1), 149–165.

Bhutiyani, M., Kale, V. S., & Pawar, N. (2007). Long-term trends in maximum, minimum and mean annual air temperatures across the northwestern himalaya during the twentieth century. *Climatic Change*, *85*(1), 159–177.

Bhutiyani, M. R., Kale, V. S., & Pawar, N. (2010). Climate change and the precipitation variations in the northwestern himalaya: 1866–2006. *International Journal of Climatology: A Journal of the Royal Meteorological Society*, *30*(4), 535–548.

Bisht, D. S., Chatterjee, C., Raghuwanshi, N. S., & Sridhar, V. (2018). Spatio-temporal trends of rainfall across indian river basins. *Theoretical and applied climatology*, *132*(1), 419–436.

Bisht, D. S., Sridhar, V., Mishra, A., Chatterjee, C., & Raghuwanshi, N. S. (2019). Drought characterization over india under projected climate scenario. *International Journal of Climatology*, *39*(4), 1889–1911.

Chowdhury, B., Goel, N., & Arora, M. (2021). Evaluation and ranking of different gridded precipitation datasets for satluj river basin using compromise programming and f-topsis. *Theoretical and Applied Climatology*, *143*(1), 101–114.

Ciabatta, L., Brocca, L., Massari, C., Moramarco, T., Gabellani, S., Puca, S., & Wagner, W. (2016). Rainfall-runoff modelling by using sm2rain-derived and state-of-the-art satellite rainfall products over italy. *International journal of applied earth observation and geoinformation*, *48*, 163–173.

Connolly, T. G., & Sluckin, W. (1971). *Introduction to statistics for the social sciences*. Springer.

Das, L., Dutta, M., Mezghani, A., & Benestad, R. E. (2018). Use of observed temperature statistics in ranking cmip5 model performance over the western himalayan region of india. *International Journal of Climatology*, *38*(2), 554–570.

Dimri, A., & Dash, S. (2012). Wintertime climatic trends in the western himalayas. *Climatic Change*, *111*(3), 775–800.

Dimri, A., & Ganju, A. (2007). Wintertime seasonal scale simulation over western himalaya using regcm3. *Pure and applied Geophysics*, *164*(8), 1733–1746.

Dimri, A. P. (2012). Atmospheric water budget over the western Himalayas in a regional climate model. *Journal of Earth System Science 2012 121:4*, *121*(4), 963–973.

Dimri, A. P., Niyogi, D., Barros, A. P., Ridley, J., Mohanty, U. C., Yasunari, T., & Sikka, D. R. (2015). Western Disturbances: A review. *Reviews of Geophysics*, *53*(2), 225–246.

Dimri, A. P., Yasunari, T., Kotlia, B. S., Mohanty, U. C., & Sikka, D. R. (2016). Indian winter monsoon: Present and past. *Earth-Science Reviews*, *163*, 297–322.

Gershon, M., & Duckstein, L. (1983). Multiobjective approaches to river basin planning. *Journal of Water Resources Planning and Management*, *109*(1), 13–28.

Gibbons, J. D., & Chakraborti, S. (2014). *Nonparametric statistical inference*. CRC press.

Guhathakurta, P., & Rajeevan, M. (2008). Trends in the rainfall pattern over india. *International Journal of Climatology: A Journal of the Royal Meteorological Society*, *28*(11), 1453–1469.

Jain, S. K., & Kumar, V. (2012). Trend analysis of rainfall and temperature data for india. *Current Science*, (pp. 37–49).

Khan, A. R. (2001). *Searching evidence for climatic change: Analysis of hydro-meteorological time series in the Upper Indus Basin*, vol. 23. IWMI.

Kripalani, R. H., Kulkarni, A., & Sabade, S. (2003). Western himalayan snow cover and indian monsoon rainfall: A re-examination with insat and ncep/ncar data. *Theoretical and Applied Climatology*, *74*(1), 1–18.

Meher, J. K., Das, L., Akhter, J., Benestad, R. E., & Mezghani, A. (2017). Performance of cmip3 and cmip5 gcms to simulate observed rainfall characteristics over the western himalayan region. *Journal of Climate*, *30*(19), 7777–7799.

Mishra, A. K. (2015). A study on the occurrence of flood events over jammu and kashmir during september 2014 using satellite remote sensing. *Natural Hazards*, *78*(2), 1463–1467.

Morais, D. C., & de Almeida, A. T. (2012). Group decision making on water resources based on analysis of individual rankings. *Omega*, *40*(1), 42–52.

Nanda, T., Sahoo, B., Beria, H., & Chatterjee, C. (2016). A wavelet-based non-linear autoregressive with exogenous inputs (wnarx) dynamic neural network model for real-time flood forecasting using satellite-based rainfall products. *Journal of Hydrology*, *539*, 57–73.

Opricovic, S., & Tzeng, G.-H. (2004). Compromise solution by mcdm methods: A comparative analysis of vikor and topsis. *European journal of operational research*, *156*(2), 445–455.

Pai, D., Rajeevan, M., Sreejith, O., Mukhopadhyay, B., & Satbha, N. (2014). Development of a new high spatial resolution (0.25× 0.25) long period (1901-2010) daily gridded rainfall data set over india and its comparison with existing data sets over the region. *Mausam*, *65*(1), 1–18.

Palazzi, E., Von Hardenberg, J., & Provenzale, A. (2013). Precipitation in the hindu-kush karakoram himalaya: observations and future scenarios. *Journal of Geophysical Research: Atmospheres*, *118*(1), 85–100.

Papalexiou, S. M., Rajulapati, C. R., Clark, M. P., & Lehner, F. (2020). Robustness of cmip6 historical global mean temperature simulations: Trends, long-term persistence, autocorrelation, and distributional shape. *Earth's Future*, *8*(10), e2020EF001667.

Parida, B. R., Behera, S. N., Bakimchandra, O., Pandey, A. C., & Singh, N. (2017). Evaluation of satellite-derived rainfall estimates for an extreme rainfall event over uttarakhand, western himalayas. *Hydrology*, *4*(2), 22.

Pomerol, J.-C., & Barba-Romero, S. (2000). *Multicriterion decision in management: principles and practice*, vol. 25. Springer Science & Business Media.

Rawat, S., Jose, P., Rai, S., & Hakhoo, N. (2018). Spring sanctuary development sustaining water security in the himalayan region in changing climate. In *Proc. of International Conference on Water Environment and Climate Change Knowledge Sharing and Partnership*, (pp. 151–159).

Shah, A. A. (2015). Assessing the influence of watershed characteristics on the flood vulnerability of jhelum basin in kashmir himalaya by gowhar et al., 2015. *Natural Hazards*, *77*(3), 2139–2143.

Shekhar, M., Chand, H., Kumar, S., Srinivasan, K., & Ganju, A. (2010). Climate-change studies in the western himalaya. *Annals of Glaciology*, *51*(54), 105–112.

Shrestha, A. B., Wake, C. P., Dibb, J. E., & Mayewski, P. A. (2000). Precipitation fluctuations in the nepal himalaya and its vicinity and relationship with some large scale climatological parameters. *International Journal of Climatology: A Journal of the Royal Meteorological Society*, *20*(3), 317–327.

Shukla, A. K., Ojha, C. S. P., Singh, R. P., Pal, L., & Fu, D. (2019). Evaluation of trmm precipitation dataset over himalayan catchment: the upper ganga basin, india. *Water*, *11*(3), 613.

Singh, J., Yadav, R. R., & Wilmking, M. (2009). A 694-year tree-ring based rainfall reconstruction from himachal pradesh, india. *Climate Dynamics*, *33*(7), 1149–1158.

Singh, P., & Kumar, N. (1997). Effect of orography on precipitation in the western himalayan region. *Journal of Hydrology*, *199*(1-2), 183–206.

Singh, P., Ramasastri, K., & Kumar, N. (1995). Topographical influence on precipitation distribution in different ranges of western himalayas. *Hydrology Research*, *26*(4-5), 259–284.

Singh, R., & Mal, S. (2014). Trends and variability of monsoon and other rainfall seasons in western himalaya, india. *Atmospheric Science Letters*, *15*(3), 218–226.

Srinivasa Raju, K., & Nagesh Kumar, D. (2010). *Multicriterion analysis in engineering and management*. PHI Learning Pvt. Ltd.

Srinivasa Raju, K., & Nagesh Kumar, D. (2015a). Fuzzy approach to rank global climate models. In *Proceedings of the Fifth International Conference on Fuzzy and Neuro Computing (FANCCO-2015)*, (pp. 53–61). Springer.

Srinivasa Raju, K., & Nagesh Kumar, D. (2015b). Ranking general circulation models for india using topsis. *Journal of Water and Climate Change*, *6*(2), 288–299.

Srinivasa Raju, K., Sonali, P., & Nagesh Kumar, D. (2017). Ranking of cmip5-based global climate models for india using compromise programming. *Theoretical and applied climatology*, *128*(3), 563–574.

Wu, Z., Xu, Z., Wang, F., He, H., Zhou, J., Wu, X., & Liu, Z. (2018). Hydrologic evaluation of multi-source satellite precipitation products for the upper huaihe river basin, china. *Remote Sensing*, *10*(6), 840.

Yang, T., & Hung, C.-C. (2007). Multiple-attribute decision making methods for plant layout design problem. *Robotics and computer-integrated manufacturing*, *23*(1), 126–137.